

1                   **Effect of perturbations by shoal margin collapses on the**  
2                   **morphodynamics of a sandy estuary**

3                   **W. M. van Dijk<sup>1</sup>, M. Hiatt<sup>1,2</sup>, J. J. van der Werf<sup>3</sup>, and M. G. Kleinans<sup>1</sup>**

4                   <sup>1</sup>Department of Physical Geography, Faculty of Geosciences, Utrecht University, Utrecht, The Netherlands

5                   <sup>2</sup>Department of Oceanography and Coastal Sciences, College of the Coast and Environment, Louisiana State University,  
6                   Baton Rouge, Louisiana, United States

7                   <sup>3</sup>Department of Marine and Coastal Systems, Deltares, Delft, The Netherlands

8                   **Key Points:**

- 9                   • Shoal margin collapses perturb the channel-shoal network of sandy estuaries.  
10                  • Disturbances cause long-term morphological changes.  
11                  • Disturbances amplify asymmetry and instability at channel junctions.

---

Corresponding author: Wout van Dijk, [W.M.vanDijk@uu.nl](mailto:W.M.vanDijk@uu.nl)

## Abstract

Shoal margin collapses of several  $\text{Mm}^3$  have occurred in the Western Scheldt estuary, the Netherlands, more than five times per year over the past decades. While these collapses have considerable volumes, their effects on the morphodynamics are unknown. We hypothesise that collapses dynamicise the channel-shoal interactions, which could impact the ecological functioning, flood safety and navigation in the estuary. The objective of this study is to investigate how locations, probability, type and volume of shoal margin collapse affect the channel-shoal morphodynamics. We implemented an empirically-validated parameterization for shoal margin collapses and tested their effects on morphodynamics in a Delft3D schematization of the Western Scheldt. Three sets of scenarios were analyzed for near-field and far-field effects on flow pattern and channel-shoal morphology: 1) an observed shoal margin collapse of 2014, 2) initial large collapses on 10 locations, and 3) continuous collapses predicted by our novel probabilistic model over a time span of decades. Results show that single shoal margin collapses only affect the local dynamics in longitudinal flow direction and dampen out within a year for typical volumes, whereas larger disturbances that reach the seaward or landward sill at tidal channel junctions grows. The redistribution of the collapsed sediment is determined by the direction of the strongest tidally averaged flow. We conclude that adding the process of shoal margin collapses increase the channel-shoal morphodynamics, and that in intensively dredged estuaries shoal margin oversteepen that amplifies the number of collapses, but because of dredging the natural channel-shoal dynamics are ruined.

Keywords: estuary; shoal margin collapse; channel-shoal morphodynamics; tidal bars; Western Scheldt

## 1 Introduction

The process of channel bank failure and collapses of shoal margins has been recognized in estuaries and rivers around the world [Coleman, 1969; Laury, 1971; Silvis and De Groot, 1995; Torrey, 1995; Dunbar et al., 1999; Van den Berg et al., 2002; Beinssen et al., 2014] but their effect on long-term morphodynamics remains unknown. Application of channel bank failure in a numerical morphodynamic model has been studied more often [Kleinhans, 2010; Nicholas, 2013a; Schuurman et al., 2013] and mainly focus on outer bank erosion in rivers. Channel banks can also collapse at the inner side of rivers [Nieuwboer, 2012], while collapses of shoal margin at the inner side of a bend is more often observed in estuaries because these shoals consist of fine uniform sands [Wilderom, 1972; Mastbergen and Van den Berg, 2003; Van Dijk et al., 2018]. Because of the relative large volume up to several million  $\text{m}^3$  involved. The eroded scar and associated displaced sediment in the channel perturbs the channel, affecting channel geometry, e.g., the width-depth ratio, and channel morphodynamics. In tidal systems perturbations likely propagate in both directions because of ebb or flood flow, but how far and how fast has not been studied. Connections to the rest of the channel network may also determine whether perturbations excite or dampen these processes. We hypothesize that the transverse bed slope steepens due to continuous aggradation, which makes the slopes unstable and could lead to breaching and liquefied flow slides associated to shoal margin collapses [Van den Berg et al., 2002; Van den Ham et al., 2014; Mastbergen et al., 2016; Van Dijk et al., 2018]. We also hypothesize that such morphological perturbations within the system may amplify the morphodynamics in estuaries as much as extreme events imposed in the boundary conditions. This is important because morphological models of estuaries invariably evolve towards bar-scale equilibrium [Van der Wegen and Roelvink, 2012; Dam, 2017]. This means that the channel-shoal dynamics are presently underpredicted and the question is whether that is due to internal dynamics not captured in the model or due to the steady forcing conditions on the model boundaries, or both.

62 Effects of disturbances and perturbations on morphology in rivers and estuaries have  
63 been studied in the past century. The damping and lag associated with environmental dis-  
64 turbances propagating through a system are determined by the magnitude and timescale  
65 of the event [Paola et al., 1992; Whipple and Tucker, 1999]. The nonlinear dynamics of  
66 sediment transport limits the potential to record and pass on physical environmental dis-  
67 turbances and perturbations [Jerolmack and Paola, 2010]. Such disturbances for fluvial  
68 systems have been subdivided into four categories [Schuurman et al., 2016a]: (i) exter-  
69 nal temporal perturbation of the upstream inflow, (ii) external spatial perturbation, e.g.  
70 along the outer channel banks, (iii) external perturbation at the downstream boundary,  
71 and (iv) internal perturbations within the reach. Shoal margin collapses fall within the  
72 fourth group of disturbances as sediment is eroded from the shoal within the estuary sys-  
73 tem. Bank erosion results in local widening of the system [Khan and Islam, 2003; Ash-  
74 worth and Lewin, 2012], and outer bank erosion is linked to bar (shoal) dynamics, as the  
75 eroded sediment is a source for bars [Xu, 1997; Ahktar et al., 2011; Van de Lageweg et al.,  
76 2014]. The role of eroding bars, i.e., shoals, on the morphodynamics remains unknown.  
77 Numerical models show that erodible floodplains result in major local braidplain widen-  
78 ing of rivers [Nicholas, 2013b], while Schuurman et al. [2016a] found that self-generated  
79 disturbances propagate through the network of bars, branches and bifurcations in braided  
80 rivers. Disturbances trigger development of asymmetrical division of discharge and sed-  
81 iment through the branches. The effect of disturbances in systems with multi-directional  
82 flow is unknown. We therefore study perturbing effects of shoal margin collapses in estu-  
83 aries, where flow is bi-directional due to tidal forcing.

84 To study the role of disturbance on the morphology of estuaries, most control is of-  
85 fered by numerical models. Numerical morphodynamic models are useful tools, but in-  
86 teraction with bank erosion processes introduces complications [Canestrelli et al., 2016].  
87 The forecasting of these interactions remains infrequently addressed because this requires  
88 coupling short term geotechnical processes and long-term morphological development.  
89 The use of curvilinear grids leads to some complications when modeling abrupt changes  
90 such as bank erosion or flow slides [Kleinhans, 2010], which might be overcome using  
91 unstructured grids and cut-cell techniques [Olsen, 2003; Canestrelli et al., 2016]. Despite  
92 successes in including bank erosion processes [Darby et al., 2002; Simon and Collinson,  
93 2002; Kleinhans, 2010], erodible floodplains mainly experience outer bank erosion pro-  
94 cesses [Nicholas, 2013a,b; Schuurman et al., 2013, 2016b], while flow slides such as liq-  
95 uefaction or breaching processes that also occur on the inner side of bends in estuaries are  
96 under-represented. However, their potential effects are considerable: a single shoal margin  
97 collapse can displace several  $\text{Mm}^3$  within a single tide, such as observed for the collapse  
98 in 2014 in the Western Scheldt [Van Schaick, 2015; Mastbergen et al., 2016; Van den Berg  
99 et al., 2017; Van Dijk et al., 2018].

100 Shoal margin collapses through flow slides often occur suddenly, which makes them  
101 difficult to predict in current numerical morphodynamic models, such as Delft3D. Lique-  
102 fied flow slides and breaching occur at sufficiently high and steep slopes, but there is a  
103 difference in the sediment properties between these two types of flow slides [Van den Ham  
104 et al., 2014]. Liquefaction requires loosely packed, non-lithified, and water-saturated sand  
105 or silt, whereas breaching requires the presence of a sufficiently large body of densely  
106 packed fine sand or silt [Van den Ham et al., 2014]. These processes are studied by var-  
107 ious models but not implemented in a numerical morphodynamic model. Van den Ham  
108 et al. [2014] argued that these theoretical liquefaction and breaching models quantify the  
109 relative influences of channel geometry and soil parameters but the reliability of the es-  
110 timated probability remains limited. Therefore, Van den Ham et al. [2014] proposed a  
111 semi-empirical model that predicts the probability of shoal margin collapses on profiles,  
112 which was modified and extended for application on spatial bathymetry data by Van Dijk  
113 et al. [2018]. This predictor includes an empirical factor based on the frequency of his-  
114 torical flow slides in the Eastern Scheldt and Western Scheldt estuaries [Wilderom, 1979;  
115 Van Dijk et al., 2018], which is applied in this study.

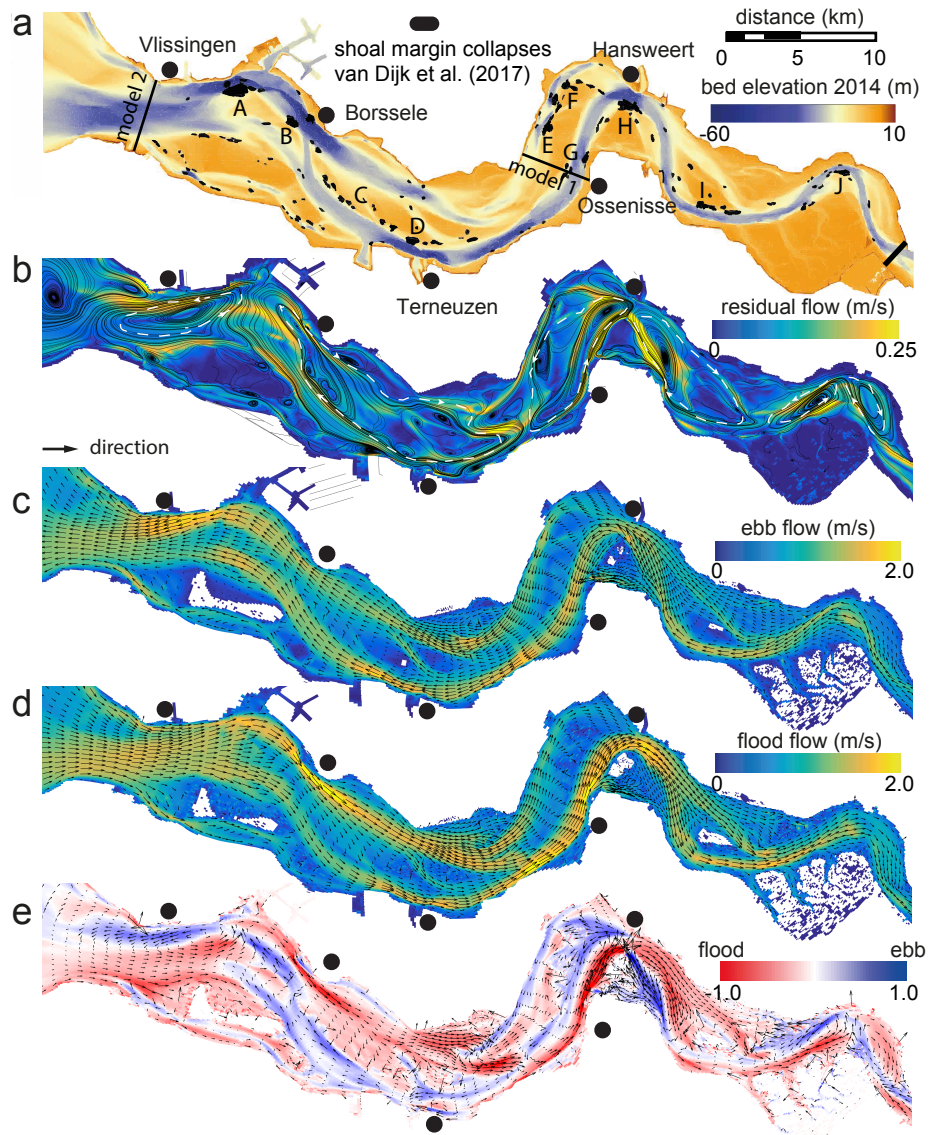
116 Our objective was to increase our understanding of the interactions between shoal  
117 margin collapses and the morphodynamics of a sandy estuary, the relevant timescales  
118 and the large-scale morphological effects. Research questions are: (i) what are the local  
119 (near-field) effects of individual shoal margin collapses, such as the observed 2014 shoal  
120 margin collapse? (ii) How do multiple shoal margin collapses affect the morphodynam-  
121 ics of the estuary (far-field effect)? Our method was to use the numerical morphodynamic  
122 model Delft3D, to implement a parametrization for shoal margin collapses in a calibrated  
123 model and to study how disturbances, such as multiple collapses, propagate and change  
124 the channel-shoal morphodynamics of the Western Scheldt; a sandy estuary. Furthermore,  
125 we test the role of grain-size and shoal margin collapse size and location of the associated  
126 collapsed deposit on the estuarine morphodynamics. In this paper, we first give a detailed  
127 description of the study area, the method for implementation of the shoal margin collapses  
128 in Delft3D, and the tested scenarios. Then, we present the near-field and far-field effects  
129 of shoal margin collapses on the short-term as well as the long-term morphodynamics of  
130 the Western Scheldt. Finally, we discuss the model performance and the implications of  
131 persistent perturbations on a sandy estuary.

## 132 2 Study Area

133 This study focuses on shoal margin collapses in the Western Scheldt. The West-  
134 ern Scheldt is located in the southwestern part of the Netherlands and is the seaward sec-  
135 tion (60 km) of the 200 km tide-dominated Scheldt estuary. The Scheldt is a well-studied  
136 and monitored estuary [e.g., *Wang et al.*, 1999; *Winterwerp et al.*, 2000; *Bolle et al.*, 2010;  
137 *Van der Wegen and Roelvink*, 2012] that provides access to various harbors, of which the  
138 port of Antwerp (Belgium) is the largest. The Western Scheldt is characterized by a con-  
139 vergent geometry, and has well-developed system of channels and shoals (Figure 1a).

149 Channel bank failure has been recorded systematically in the Western Scheldt for  
150 the past 200 years [*Wilderom*, 1961, 1979]. Over the years, bank protection measures have  
151 been implemented to protect the channel banks and dikes of the Western Scheldt against  
152 new failures and collapses. However, these measures did not fully prevent the occurrence  
153 of shoal margin collapses [*Wilderom*, 1972]. A recent study identifies 300 shoal margin  
154 collapses between 1959-2015 [Figure 1a, *Van Dijk et al.*, 2018]. The majority of the col-  
155 lapses are found at unprotected areas. Relatively fine sediment is found in the estuary,  
156 which affects the occurrence of shoal margin collapses [*Van den Ham et al.*, 2014]. In gen-  
157 eral, the  $D_{50}$  of the channel bed varies between about 200  $\mu\text{m}$  and 300  $\mu\text{m}$ , whereas at  
158 the higher elevation areas of the shoals the sediment size is generally finer than 200  $\mu\text{m}$   
159 [*Cancino and Neves*, 1999; *De Vriend et al.*, 2011]. Additionally, a significant percentage  
160 of mud can be found in the intertidal areas [*Braat et al.*, 2017].

161 The natural development of the morphology as well as the effect of perturbations  
162 is the result of interactions between water flow, sediment transport and bed elevation.  
163 An important factor causing bi-directional flow and mean sediment transport is the tidal  
164 forcing in the Western Scheldt [*Wang et al.*, 1999]. From the mouth of the estuary to the  
165 Dutch/Belgian border, the tidal range increases from 3.5 m to 5 m [*Jeuken*, 2000]. The  
166 tidal prism at the mouth is about two billion  $\text{m}^3$  [*Wang et al.*, 1999], whereas the yearly-  
167 averaged river discharge of the Scheldt into the Western Scheldt is a negligible 120  $\text{m}^3/\text{s}$   
168 [*Cancino and Neves*, 1999; *De Vriend et al.*, 2011]. The Western Scheldt has several recir-  
169 culation zones of sediment through the ebb and flood channels, which enclosed the inter-  
170 tidal flats [Figure 1b, *Wang et al.*, 1995; *Winterwerp et al.*, 2000]. The tidal flow is asym-  
171 metric, i.e., slower but longer ebb flows compared to flood flows, in the Western Scheldt  
172 (Figure 1c–d). The difference between the maximum flow velocity for ebb and flood il-  
173 lustrated that flood is generally stronger (Figure 1e) even in the ebb dominated channels  
174 illustrated by the tidally averaged flow (Figure 1b).



140 **Figure 1.** Overview of hydromorphodynamics in the Western Scheldt Estuary. a) Shoal margin collapse  
 141 locations plotted on a digital elevation model of 2014 [Van Dijk et al., 2018]. Seaward boundaries are indi-  
 142 cated for the two morphological model schematizations in this study. A-J indicate locations susceptible to  
 143 shoal margin collapses that are applied in the model scenario with ten initial collapses. b) Streamlines of the  
 144 tidally averaged flow of the original NeVla-Delft3D flow model showing circulation cells that correspond  
 145 largely to the macro cells indicated in white defined by Winterwerp et al. [2000] and Bolle et al. [2010]. c)  
 146 Maximum flow velocity in the ebb-direction from the NeVla-Delft3D model. d) Maximum flow velocity in  
 147 the flood-direction from the NeVla-Delft3D model. e) Difference between the maximum ebb and maximum  
 148 flood velocity showing flood dominance in the main channels.

### 3 Model description and methods

#### 3.1 Model setup and boundary conditions

In this study, we used two Delft3D schematizations that are both based on the NeVla-Delft3D model of the Scheldt estuary, which includes the upstream Flemish branches of the estuary, the Western Scheldt and part of the North Sea. The NeVla model is a state-of-the-art numerical model that has been optimized for hydrodynamics [Maximova *et al.*, 2009a,b,c; Vroom *et al.*, 2015] and morphology [Grasmeijer *et al.*, 2013; Schrijvershof and Vroom, 2016]. To study the effect of shoal margin collapses we focused on the Western Scheldt part of the NeVla model. Therefore, two nested models were produced from the NeVla-Delft3D model for reducing the computational time. The first nested model boundaries (model 1) were located around the tidal flat of Walsoorden (see boundaries in Figure 1a), which was used to study the morphodynamic response of the 2014 shoal margin collapses and the sensitivity to collapse sizes, grain-size of the collapsed material, and location of the collapsed deposits [see also Van Schaick, 2015]. Van Schaick [2015] validated the water level and discharge from the nested model with the NeVla-Delft3D model, and concluded that the errors were small enough to be neglected for the area of interest. The second nested model boundaries (model 2) include the Western Scheldt from the mouth at Vlissingen to the Belgian border (see seaward boundaries in Figure 1a), which was used for testing the effect of various shoal margin collapse locations as well as the effect of multiple shoal margin collapses in the Western Scheldt over time. The downstream boundary was chosen at the smallest but deepest part of the Western Scheldt to limit boundary effects. A single neap-spring cycle shows that the tidally averaged flow of this model (Supplementary Figure 4b) is comparable with the outcome of the full NeVla-Delft3D model (Figure 1b), except for small variation at the seaward end.

The nested model consists of a curvilinear grid with various grid sizes. The boundary conditions include a water level fluctuation due to tides at the seaward boundary and a current at the landward boundary. Sediment fraction was uniform with a median grain-size of 200  $\mu\text{m}$ . For simplification of the boundary conditions, boundary conditions were selected from a single spring-neap tide cycle of January 2013 (about 14 days) and repeated for a 2 year period. Furthermore, we excluded the wind direction and magnitude from the NeVla model to reduce computational time as the effect of wind is negligible within the Western Scheldt. The roughness field in the model is defined in Manning  $n$  and is variable over the model domain [Maximova *et al.*, 2009a,b,c; Vroom *et al.*, 2015], which was 0.022  $\text{s}\cdot\text{m}^{-1/3}$  for the eastern part, 0.027  $\text{s}\cdot\text{m}^{-1/3}$  for the western part and 0.028  $\text{s}\cdot\text{m}^{-1/3}$  for the Verdrongen Land van Saeftinghe. The bed consisted of erodible and non-erodible layers [Gruijters *et al.*, 2004], the non-erodible layers are formed due to former deposits that are hardly erodible [Dam, 2013], and therefore the sediment thickness varies within the Western Scheldt model (see Supplementary Figure 1). Because sediment transport was calculated by Van Rijn [2007a,b], the bedload and suspended load transport could be distinguished.

#### 3.2 Transverse bed slope and morphological factor

The Delft3D model (version FLOW 6.01.07.3574, 2 April 2014) has been applied in many scientific projects to compute hydrodynamics, sediment transport, and morphodynamics [Roelvink, 2006; Deltares, 2009; Crosato and Saleh, 2011; Van der Wegen and Roelvink, 2012; Schuurman *et al.*, 2013, 2016a; Van Dijk *et al.*, 2014]. In this study, we applied a 2D depth-averaged flow field, which meant that the effect of helical flow driven by flow curvature on bed shear-stress direction were parametrized [Schuurman *et al.*, 2013]. The parametrization affected the transverse bed slopes at the shoal margins, which influenced the moment that shoal margin collapses were predicted. Therefore, we performed a sensitivity analysis to determine how the sediment transport direction affects the slopes for various  $\alpha_{bn}$  (see Supplementary Text S1). To reduce computational time, Delft3D in-

256

**Table 1.** Model scenarios

Scenario	Model	Test	duration	comments
1	1	2014 collapse	1 year	see <i>Van Schaick</i> [2015]
2	2	initial 10 collapses	40 years	see locations Figure 1a
3	2	yearly collapses	40 years	rule based on <i>Van Dijk et al.</i> [2018]
Sensitivity scenarios				
collapse size	1	100,000 m <sup>3</sup> vs. 1,000,000 m <sup>3</sup>	1 year	see Supplementary
grain size	1	100 $\mu\text{m}$ vs. 200 $\mu\text{m}$ vs. 300 $\mu\text{m}$	1 year	see Supplementary
$\alpha_{bn}$	1	1.5 vs. 30	1 year	see Supplementary

cludes a morphological acceleration factor  $M$ . We performed a sensitivity analysis determine what effect  $M$  has on the morphology of the estuary (see Supplementary Text S1). According to these both analyses we set  $\alpha_{bn}$  to 30 and  $M$  to 20 as a default, so that that realistic dimensions of the slopes for long-term simulations were maintained (see Supplementary Figure 2).

### 3.3 Model scenarios and sensitivity

We assessed the effect of shoal margin collapses on the morphodynamics of a sandy estuary in three scenarios (see Table 1).

The first scenario was to understand the near-field effect of a single shoal margin collapse, such as the observed 2014 shoal margin collapse at the tidal flat of Walsoorden. Various sensitivity scenarios (see Supplementary Text S3) were applied to study the effect of the shoal margin collapse size, location of the collapsed deposits, and grain-size of the deposits. The collapsed size was tested because of the variation in size observed by *Van Dijk et al.* [2018] as well as its locations. Furthermore, the grain size of the deposited material was varied as the grain-size distribution in the field showed minor variation between 100  $\mu\text{m}$  on the shoals and 300  $\mu\text{m}$  in the channel [*Mastbergen et al.*, 2016]. This scenario and sensitivity tests were conducted on only the eastern part of the Western Scheldt (see seaward boundary of model 1 in Figure 1a).

The second scenario included a model run with initially shoal margin collapses of 1,000,000 m<sup>3</sup> at various locations within the Western Scheldt to test the far-field effect on the morphodynamics for the various location on a long-term (40 years). The various locations corresponded to observed shoal margin collapse locations described in *Van Dijk et al.* [2018] (Figure 1a).

The third scenario tested the role of multiple shoal margin collapses over a period of 40 years. These collapses were controlled by the implementation of shoal margin collapse rules in a Matlab environment as described in next section. Each of the three scenarios was compared to a control run without shoal margin collapses, so that natural variation of the morphodynamics could be excluded. These last two scenarios were applied on a different nested model (see Table 1), which includes the Western Scheldt from Vlissingen to the Belgian border (see seaward boundary of model 2 in Figure 1a).

### 3.4 Shoal margin collapses

Overestimating the transverse bed slope effect in the morphodynamic model [*Baar et al.*, 2018], causing more downslope sediment transport, may be necessary to flatten the morphology and compensate for subgrid bank erosion processes that usually does not oc-

cur in the numerical models [Grenfell, 2012; Schuurman et al., 2013; Van Dijk et al., 2014] but reduces morphodynamics within the model. Including the process of shoal margin collapses into a morphodynamic model might increase the morphodynamics. Currently, bank erosion is implemented by coupling horizontal bank retreat to bed degradation in Delft3D. Bank erosion occurs between an inundated grid cell and a dry grid cell, and thus is not restricted to the outer banks. Incision of the inundated grid cell could be equally divided over both grid cells or solely on the dry cell, so that the dry cell was lowered and the bank eroded [Schuurman et al., 2016b; Mastbergen and Schrijvershof, 2016]. This process is continuous until the grid cell becomes inundated, but shoal margin collapses may occur suddenly at growing shoals that become less inundated.

The first step towards implementation of shoal margin collapses was the determination of locations that were unstable. In previous work, Van Dijk et al. [2018] modified a forecasting method of Van den Ham et al. [2014] for determining shoal margin collapse locations based on bathymetry data. Van Dijk et al. [2018] tested the accuracy of the prediction by corresponding higher probabilities with observed shoal margin collapse locations and showed the validity of the method. In this study, we applied this forecasting method into the morphodynamic model Delft3D. The first step towards determining shoal margin collapse locations was to determine the shoal margins. The shoal margins were determined by fitting a linear regression for the median bed elevation along the estuary channel [see also Leuven et al., 2018a; Van Dijk et al., 2018]. Elevation above the regression line was determined as shoal and below as channel. The boundary of the shoal was then extracted to determine the shoal margin. Subsequently, shoal margin collapse frequencies,  $F_{SC}$ , were calculated [adapted from Van Dijk et al., 2018] as follows

$$F_{SC} = \left[ \left( \frac{H}{11} \right)^{2.5} \left( \frac{9.5}{\cot \alpha} \right)^5 \right] \frac{SC_{avg}}{L_{sm}} \quad (1)$$

where  $H$  is the elevation of the local maximum between the center and the deepest part within a window size of 300 by 300 m on a 20 by 20 m interpolated grid of the bed elevation.  $\alpha$  is the corresponding angle to  $H$ ,  $SC_{avg}$  is an empirical value based on the average number of collapses observed per year [5.3 for the Western Scheldt, Van Dijk et al., 2018], and  $L_{sm}$  is the measured total length of shoal margins [300 km for the Western Scheldt, Van Dijk et al., 2018]. The form of equation 1 allowed frequency to be higher than 1, which was prevented by a transformation, namely a Poisson process, of the frequency into a probability ( $P_{SC}$ ):

$$P_{SC} = 1 - e^{-F_{SC}} \quad (2)$$

Van Dijk et al. [2018] found that at a probability threshold ( $P_{SC}$ ) value of  $10^{-4}$  the true positive rate, defined as the number of cells that had shoal margin collapses in both the predictive probability and observed collapses divided by the number of observed locations of collapses, was almost 0.5, while the remaining identified locations had a low false positive rate, defined as the number of cells that had shoal margin collapses in the predictive probability but no observations of collapses divided by the number of cells with no shoal margin collapse observations. Because multiple locations at the shoal margin could have a probability value greater than the given threshold of  $10^{-4}$ , we limited the number of collapses to a maximum of 1 per tidal flat (shoal margin) per time-interval. The time-interval was set to 1 morphological year. Eroding shoal margins were excluded, because these were already eroding by continuous channel migration, and collapses mostly occurred suddenly at vertical aggradational margins. Eventually, the highest probability above the critical probability of  $10^{-4}$  was used to select the location of the shoal margin collapse per tidal flat. These slopes collapsed to a post-event slope whilst conserving mass, in which the size and geometric shape of the collapses followed a 1/3 ellipsoid according to the

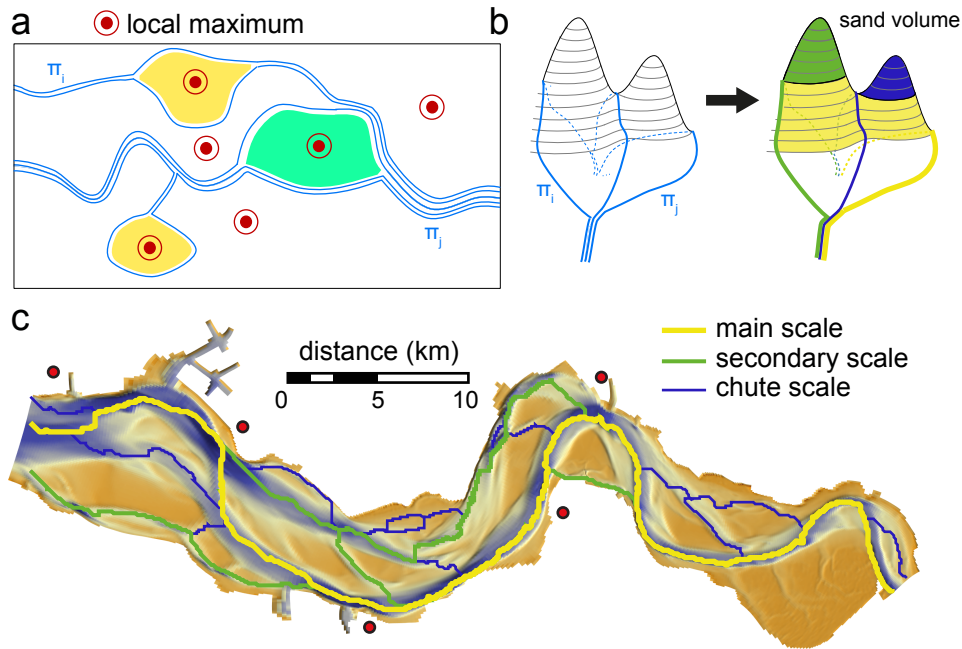
309 analysis of *Van Dijk et al.* [2018] of the geometric shape of the erosion scar (see supple-  
310 mentary Text S2).

### 311 3.5 Data analyses

312 The Delft3D model outcomes were analyzed for near-field and far-field effects, i.e.,  
313 local and estuary scale. The analysis of the near-field effects on a short-term were mainly  
314 conducted on the 2014 shoal margin collapses, whereas for the Western Scheldt model  
315 (second and third scenario) the far-field effect on the long-term morphology was analyzed.  
316 For the near-field effect we analyzed the distribution of the collapsed sediment by labeling  
317 the collapsed deposit as a second sediment fraction with the same grain-size in the model.  
318 The model outcomes were also analyzed by looking at the Digital Elevation Model (DEM)  
319 of Difference (DoD) between a run with the collapse and a control run. The distribution  
320 of the collapsed sediment was plotted in time-space diagram for the cross flow-direction  
321 as well as longitudinal flow-direction. Furthermore, the width-averaged bed elevation was  
322 calculated and compared between the runs with and without collapses.

323 For analyzing the shoal margin collapse effects, the tidally-averaged flow and mean  
324 sediment transport were calculated over a spring-neap tide cycle. Eventually, the tidally-  
325 averaged flow and mean sediment transport were summarized by plotting the vectors for  
326 determining the net direction of the flow and of the sediment transport. For the second  
327 scenario, i.e., the 10 initial collapses of 1,000,000 m<sup>3</sup>, the sediment transport direction  
328 was determined for the spring-neap tide cycle at the location of the collapse as well as for  
329 the location of the deposit. The smoothing of the bed elevation was determined by calcul-  
330 ating the average bed elevation within the collapse as well as for the associated deposit  
331 location and compared to a rose diagram for the sediment transport direction.

332 We were specifically interested in the role of shoal margin collapses on the channel-  
333 shoal morphodynamics. Therefore, we used an existing tool to characterize the channel  
334 network. This network tool has been applied to braided rivers to determine the drainage  
335 network, so it includes channel bifurcations [*Kleinhans et al.*, 2017]. The tool uses the lo-  
336 cal lows of the channel bed to determine its lowest path. Specifically, the tool determines  
337 minimums, maximums and saddle points and connect the minimums through a saddle  
338 point, according to a descending quasi Morse-Smale complex [*Kleinhans et al.*, 2017].  
339 The lowest path was then combined with striation, i.e., an ordered set of non-crossing  
340 paths, that subdivide the lowest path  $\pi$  into two parts around a maximum (green area in  
341 Figure 2a). Afterwards, the path is again divided into two parts around another maximum  
342 in that path (yellow areas in Figure 2a), and so on. To determine the scale of the channel  
343 network, a sand function ( $\delta$ ) is defined that represent the volume of sediment that has to  
344 be removed before two channels become one in the network, which volume is calculated  
345 from the elevation above the saddle point [Figure 2b *Kleinhans et al.*, 2017]. This made  
346 it possible to compute graphs representing the channel network, consisting of the lowest  
347 paths for various scales (Figure 2c). We named the various channel networks scales like  
348 the names used in the Western Scheldt [*Jeuken*, 2000], however, the identified channel net-  
349 work by the tool is not equal to the observations. The largest scale is the referred as the  
350 main channel, the next scale is referred as the secondary channel, and the third scale is  
351 referred as chute channel, which in nature is referred to channels that connect the main  
352 with the secondary channel. After identifying the channel network for the various network  
353 scales, we analyzed the channel dimensions for the various network scales and between  
354 the model outcomes of the three long-term simulation scenarios.



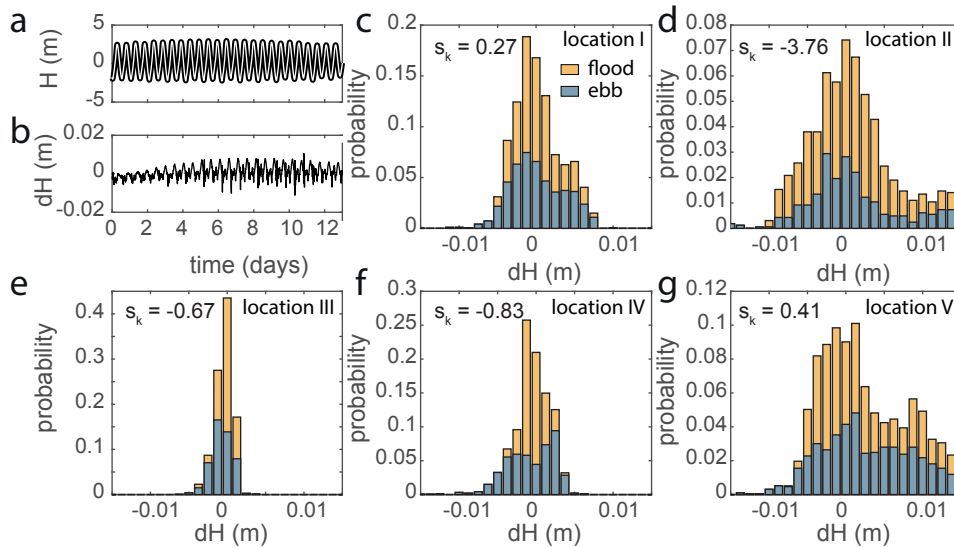
355 **Figure 2.** Illustration of the network identification tool. a) Example of how identification of the minimum,  
 356 maximum and saddle point according to the Morse-Smale complex combined with striation analysis results  
 357 in a channel network of multiple channels ( $\pi$ ). b) Identification of different scales for the lowest paths ( $\pi$ )  
 358 according to a sand function volume. The example indicates three scales, from the smallest sand volume up  
 359 to the largest sand volume, in which the largest scale is referred to as the main channel scale, followed by  
 360 the secondary channel scale and the chute channel scale. c) Example network in the Western Scheldt for the  
 361 initial bathymetry.

## 362 4 Results

### 363 4.1 The 2014 shoal margin collapse

#### 364 4.1.1 Hydrodynamics

365 Water level changes around the shoal margin collapse location as well as around  
 366 associated deposits in the channel compared to the control run as result of the changes  
 367 in bed elevation and associated bed friction. Over time, the water level fluctuates within  
 368 1 cm between both simulations under the same boundary conditions (Figure 3a, b). The  
 369 main difference between the simulation with a collapse and the control run is found in  
 370 transverse direction of the collapse (Figure 3c,d & g), whereas in longitudinal direction  
 371 there is less change in the water level compared to the control run (Figure 3e, f). The  
 372 largest difference in the water level change is observed at the scar of the shoal margin col-  
 373 lapse (Figure 3d), which is inundated for a shorter time without the collapse because of  
 374 the higher elevation. The water level difference between the two runs does not dominantly  
 375 show lower or higher water levels around the collapse. The skewness of the change in the  
 376 water level distribution indicates that water level increases for the shoal margin collapse  
 377 deposit locations (Figure 3c, g), whereas the other locations show a decrease of the water  
 378 level. The distribution of the water level changes varies between ebb and flood conditions  
 379 for locations landward and seaward of the shoal margin collapse (Figure 3e, f), indicating  
 380 that water level increases for flood conditions seaward and decreases for flood conditions  
 381 landward.

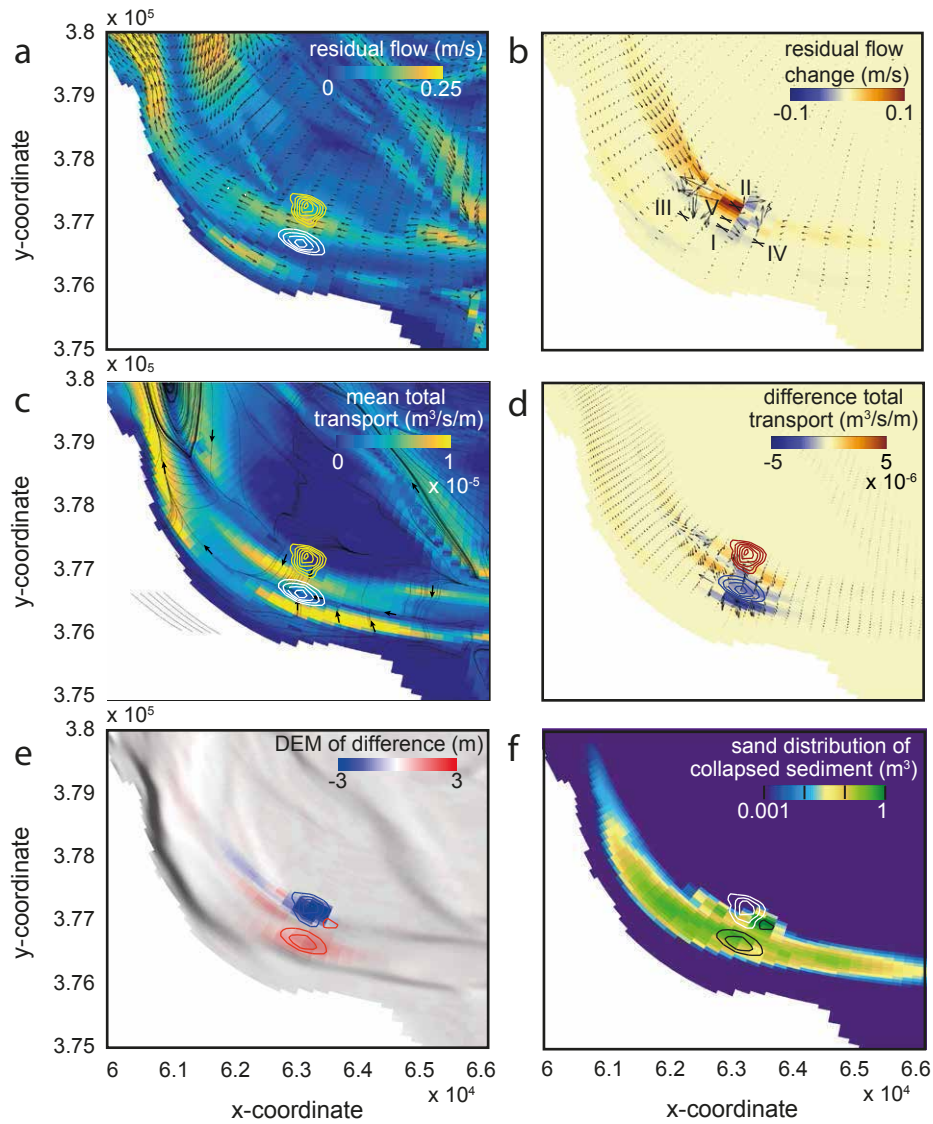


382 **Figure 3.** Changes in the water elevation relative to the control run at the 5 surrounding grid cells of the  
 383 shoal margin collapse of 2014 (locations in Figure 4b). a) Water level at location of the collapsed sediment  
 384 deposit (location I) for a simulation without (thick black line) and with the 2014 shoal margin collapse (thin  
 385 white line on top). b) Difference in water surface elevation at the deposited collapsed sediment is within 1 cm.  
 386 Positive values indicate water level rise following the collapse. c) Distribution of water level change shows a  
 387 slight increase in the water level. Here,  $s_k$  indicates if the distribution is skewed to the left (negative) or right  
 388 (positive) from the mean of the distribution, where the mean is 0 m for all distributions. The two different col-  
 389 ours show differences between ebb and flood conditions but no systematic lower or higher water levels. d) The  
 390 water level generally decreases. e) Seaward there is a slight difference in the water level, whereas f) landward  
 391 there is more difference as in generally the water level lowers. g) Water level increases on the shoal margin.

392 Besides small changes in the water level around the collapse, we also observed small  
 393 changes in the tidally averaged flow direction along the shoal margin. The control run  
 394 shows that tidally averaged flow direction (Figure 4a) is comparable with the original  
 395 NeVla-Delft3D model (Figure 1b) around the shoal margin of the ‘Plaat van Walsoorden’.  
 396 The simulation shows that the tidally averaged flow is affected by the shoal margin col-  
 397 lapse, but mainly around the location of the collapse. The overall tidally averaged flow re-  
 398 mains similar for both simulations but there is a slight change in direction and magnitude  
 399 of the tidally averaged flow. For example, flow velocity increases along the shoal margin  
 400 with 0.1 m/s because of the collapse (Figure 4b).

#### 412 4.1.2 Sediment transport

413 Sediment transport is calculated with the *Van Rijn* [2007a,b] equation, which sepa-  
 414 rates the bedload from suspended load transport. The mean total transport follows the  
 415 direction of the tidally average flow. In the north side of the channel the total transport  
 416 is towards the center, whereas in the center of the channel the transport is ebb dominated  
 417 and south flood dominated (Figure 4c). The total sediment transport is the result of bed-  
 418 load as well as suspended sediment transport. The mean bedload transport follows the  
 419 direction of the tidally averaged flow (Supplementary Figure 5a), which indicates a clear  
 420 distinction in ebb and flood directed transport. The north side of the channel, along the  
 421 shoal, is mainly ebb directed, while the south side is flood directed. The mean suspended  
 422 sediment transport does not follow the tidally averaged flow direction at all locations, es-



401 **Figure 4.** Hydromorphodynamics at a single shoal margin collapse after 1 year compared with a run with-  
 402 out the collapse. a) The tidally averaged flow modeled for the control run shows ebb-dominated flow along  
 403 the shoal margin collapse of 2014 (yellow), while at the deposit (white) it is around zero. The contour lines  
 404 were plotted at 1 m elevation intervals. b) Tidally averaged flow increases along the shoal margin seaward  
 405 of the collapse and slows down at the collapse. Crosses numbered I-V are the locations for water elevation  
 406 shown in Figure 3. c) The mean total transport is ebb-dominated at the shoal margin (note vectors), but, as  
 407  $\alpha_{bn} = 30$ , as a large transverse component into the channel along the Tidal flat of Walsoorden. d) The to-  
 408 tal transport reduces around the shoal margin collapse. e) The deposited sediment is spread only directly  
 409 landward and seaward of the collapse, whereas the eroded collapse location remains unfilled. f) Sediment is  
 410 dominantly spread in seaward direction in the channel along the vectors of the mean total sediment transport  
 411 (see Figure 4c).

423 pecially in the main channel south of the tidal flat of Walsoorden (Supplementary Figure  
 424 5b). Here, a direction is observed opposite from the bedload transport, in which north of  
 425 the channel transport is mainly flood directed, while south is ebb directed. We suspect  
 426 that this is the result of the transverse bed slope predictor, which has no effect on the sus-  
 427 pended sediment transport.

428 The direction of the sediment transport is more transverse compared to model runs  
 429 with a  $\alpha_{bn}$  of 1.5 (Supplementary Figure 5d), but the magnitude in longitudinal direc-  
 430 tion is comparable, which is important regarding the migration of the perturbation of the  
 431 shoal margin collapse on the morphodynamics of the estuary. Because of the change in  
 432 the tidally averaged flow due to the shoal margin collapse, sediment transport direction  
 433 and magnitude is affected as well. For example, the run with the shoal margin collapse  
 434 of 2014, the mean total transport, i.e., the effective sediment transport, reduces by a value  
 435 that is 80% of the mean total transport for the control run at the location where sediment  
 436 from the collapse deposited (Figure 4d). The mean total transport, however, increases  
 437 along the shoal margin by 15% and especially increases within the shoal margin collapse.  
 438 Less sediment transport means that erosion of the deposited sediment will take longer,  
 439 whereas the increase in sediment transport would increase erosion along the shoal margin.

#### 440 **4.1.3 Morphodynamics**

441 By comparing the run with the 2014 shoal margin collapse with the control run,  
 442 changes in the morphology between the runs can be ascribed specifically to the shoal mar-  
 443 gin collapse because the natural variation in the morphology was excluded. The DEM of  
 444 difference (DoD) shows that the bed elevation in the channel landward as well as seaward  
 445 of the collapsed deposit is raised after about 1 year morphological time, whereas the loca-  
 446 tion of the deposit is lowered from the start of the simulation (Figure 4e). This suggests  
 447 smoothing of the profile after the collapse. The shoal margin collapse is still visible as it  
 448 remains lower compared to the control run, and the process of sedimentation is less com-  
 449 pared to the erosion that smooths the channel.

450 The difference in bed elevation shows the changes between the two runs but does  
 451 not show how sediment from the collapse is distributed. Therefore, in the simulation with  
 452 the 2014 shoal margin collapse the collapsed sediment is labeled, so that the spreading  
 453 of the sediment could be traced. Figure 4f shows the distribution of the sediment from  
 454 the collapse within the main channel at the ‘Plaat van Walsoorden’. Large portions are  
 455 deposited at the sides of the original location, which corresponds with the DoD. The dis-  
 456 tribution of the collapsed sediments is spread over a larger area in landward as well as  
 457 seaward direction, which is less clear from the DoD because of the limited changes in bed  
 458 elevation. Suspended sediment is supposed to travel a longer distance leading to distribu-  
 459 tion over a larger area, whereas bedload sediment affected more the bed elevation. Despite  
 460 the transport in both directions there is a dominant distribution of the tracer sediment in  
 461 ebb direction (Figure 4f).

#### 462 **4.2 Shoal margin collapse scenarios to determine sensitivity**

463 In the supplementary we elaborate more in detail on the sensitivity of various sce-  
 464 narios, such as the size of the collapse, the location of the collapsed sediment and the  
 465 role of grain-size. The results from this analysis is that migration rate of the disturbance  
 466 is hardly affected by the collapsed volume, and that only large collapses,  $> 100,000 \text{ m}^3$   
 467 affect the far-field morphodynamics (Supplementary Figure 7). The location of the col-  
 468 lapsed deposits along the Western Scheldt determines the dominant direction of the distur-  
 469 bance, which corresponds to the tidally averaged flow direction. Collapses that occurred  
 470 more landwards are less reworked and transport direction is dominantly in seaward direc-  
 471 tion (Supplementary Figure 7). Model outcomes for different  $\alpha_{bn}$  values do not change  
 472 longitudinal displacement of the disturbance but do effect the distribution of the sedi-

473 ments in transverse direction (Supplementary Figure 5c, d). Besides the location of the  
 474 collapsed deposit, also the grain-size of the deposit determines the direction of the distur-  
 475 bance. Finer material follows the same dominant longitudinal direction as the  $200\mu\text{m}$ , but  
 476 settles more at the sides of the channel, whereas coarse material follows not dominantly  
 477 the tidally averaged flow but the strongest flow direction, while only the sediment in the  
 478 deepest part of the channel is entrained (Supplementary Figure 6).

479 We conclude that shoal margin collapses locally affect the morphodynamics of the  
 480 Western Scheldt leading to changes in sediment transport direction and morphology within  
 481 the first year after occurrence, and that size and location of the collapse matters. In the  
 482 next sections, we will test how these local collapses affect the regional morphodynamics  
 483 of the Western Scheldt, especially what the effect is of multiple collapses over a period of  
 484 40 years, and if this will dynamicise the system as we hypothesized.

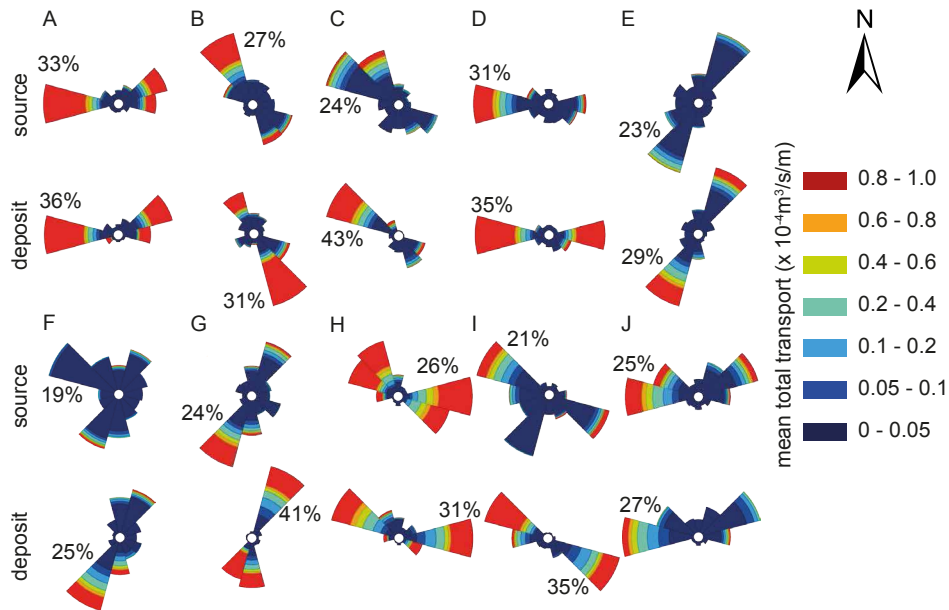
### 485 **4.3 Shoal margin collapses in the Western Scheldt**

486 Five shoal margin collapses occur per year at several locations within the West-  
 487 ern Scheldt, ranging from very small collapsed volumes of  $20,000\text{ m}^3$  up to volumes of  
 488  $3,000,000\text{ m}^3$ . The 2014 shoal margin collapse is one of the larger collapses that occurred  
 489 but its effect in isolation on the estuary morphodynamics is limited. The historical anal-  
 490 ysis of *Van Dijk et al. [2018]* shows several locations that are susceptible to shoal margin  
 491 collapses (Figure 1a). Here, we first identify how much effect each individual location  
 492 susceptible to collapse (see specific collapsed locations in Supplementary Figure 4a) has  
 493 on the morphodynamics, and second we apply our shoal margin collapse method to test if  
 494 multiple yearly collapses over time would dynamicise the Western Scheldt estuary.

#### 495 **4.3.1 Multiple initial collapses**

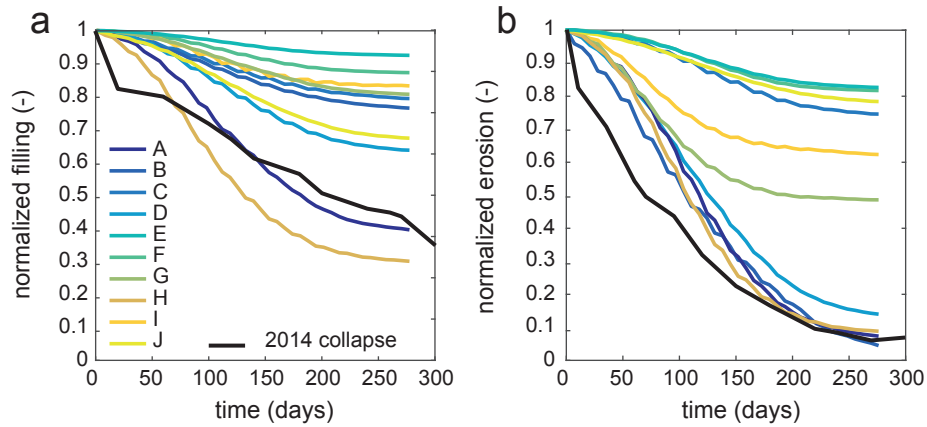
496 The Western Scheldt schematization (model 2) is used to test the long-term effect of  
 497 multiple shoal margin collapses on the morphodynamics of the system for 40 years. In the  
 498 first scenario, 10 shoal margin collapses of a volume of  $1,000,000\text{ m}^3$  are initially added  
 499 to the bed elevation of the Western Scheldt. Examining the sediment transport direction  
 500 for the various locations shows that sediment transport direction and rate varies. Most lo-  
 501 cations show sediment transport in two dominate directions corresponding with the ebb  
 502 and flood current (Figure 5). Furthermore, at most locations the sediment transport is less  
 503 for the location where the collapse originated compared to the location where it deposited.  
 504 There are some exceptions, which is the result because of the collapse occurs under water,  
 505 e.g., the ‘Spijkerplaat’ (location A). Perpendicular to the ebb and flood flow sediment is  
 506 transported on the transverse bed slope, probably because of the relative high  $\alpha_{bn}$  of 30,  
 507 which is specifically observed at the ‘Molenplaat’ and ‘Plaat van Walsoorden’ (locations F  
 508 and I).

514 The sediment transport magnitude determines the rate that the shoal margin collapse  
 515 is filled and the collapsed sediment is eroded from the main channel. The net sediment  
 516 transport varies between ebb and flood flow as well as between spring and neap tidal cy-  
 517 cles. The net sediment transport for neap tidal cycle is about  $5 \cdot 10^5\text{ m}^3$  and for spring tidal  
 518 cycle about  $5 \cdot 10^6\text{ m}^3$  within the Western Scheldt estuary. The net sediment transport is  
 519 slightly higher during rising tide than for falling tide. Locations with the highest sediment  
 520 transport rates, such as the ‘Spijkerplaat’ West and ‘Ossensisse’ (locations A and H), show  
 521 faster infilling of the shoal margin collapse (Figure 6a). The collapse at the ‘Plaat van  
 522 Walsoorden’ (location I) is less filled, which is also observed for the first scenario model  
 523 outcome of the 2014 collapse, and can be associated to lower sediment transport rates,  
 524 whereas observations showed faster filling of the scar (Figure 6a). Sediment transport rate  
 525 also determines the rate of erosion of the collapsed sediment. In general, the erosion is  
 526 faster than the infilling except for the deposits in the secondary channels (Figure 6b), e.g.,  
 527 the ‘Brouwersplaat’ (E) and ‘Molenplaat’ (F).



509 **Figure 5.** Total sediment transport magnitude and direction for various collapse locations (see locations  
 510 in Figure 1a) show dominantly ebb and flood flow-related directions for the first year after the collapse. At  
 511 the shoal margin collapse locations (top wind roses) less transport is calculated and at some locations a third  
 512 dominant direction is observed because of the transverse bed slope effect (see F and I). Sediment transport is  
 513 generally higher for the deposited sediment (bottom wind roses).

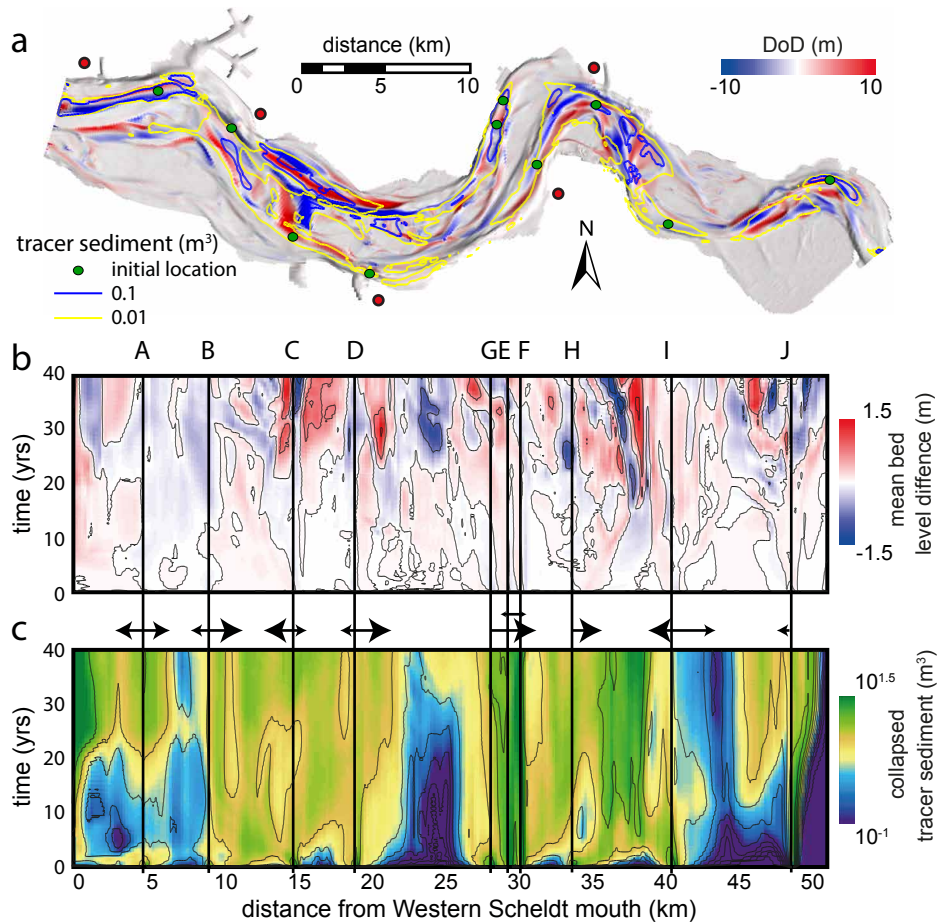
535 The sediment transport rate does affect the morphodynamics for the long-term changes  
 536 in the estuary. The bed elevation difference and tracer sediment distribution map (Figure  
 537 7a) indicates that shoal margin collapses perturb the Western Scheldt differently de-  
 538 pending on their location, which corresponds to the sediment transport direction and mag-  
 539 nitude at the collapsed locations. Major changes are observed around the shoal margin  
 540 collapse locations, when these disturbances enter areas that have less sediment transport  
 541 but are morphodynamic active and controls sediment diversion, i.e., the junctions seaward  
 542 or landward of the channel. Here, the bed elevation is not only affected in longitudinal di-  
 543 rection but also in transverse direction into connected channels (Figure 7a), i.e., effectively  
 544 following the sediment vectors. On a longer timescale, the shoal margin collapses affect  
 545 the dynamics of the system, so that a total volume change of  $4.53 \cdot 10^8 \text{ m}^3$  was observed  
 546 compared to the control run, in which less than 10% of the volume is directly the result  
 547 of the collapses. The width-averaged mean bed level difference between the two simu-  
 548 lation shows that changes excite, i.e., grow, over time (Figure 7b). At the beginning, there  
 549 is a slight difference between the runs, which was also demonstrated with the 2014 col-  
 550 lapse, but eventually the mean bed elevation across varies more than a meter (Figure 7b).  
 551 This is particularly the result of migration of the junction around location C and landward  
 552 of location H (Figure 7a). The sediment from the shoal margin collapse is mainly trans-  
 553 ported in longitudinal direction, landward as well as seaward (Figure 7a). Following the  
 554 tracer sediment along the estuary gives more insights in the dominant migrating direction  
 555 of the disturbance (Figure 7c), which vary with location but is dominantly landwards for  
 556 the seaward collapses and seawards for the more landward collapses. Changes in the bed  
 557 elevation even occur on the locations where no sediment is located that originates from  
 558 shoal margin collapse, e.g., at 25 km (Figure 7b,c).



528 **Figure 6.** Development of shoal margin collapse scar and deposit volumes at various locations for the  
 529 Delft3D simulation in the first year (see locations in Figure 1a). The shoal margin collapse of 2014, close  
 530 to modelled location I, is shown for comparison [see *Van Schaick, 2015*]. a) Filling of the scar varies with  
 531 location, but is never completed within a single morphological year. b) Deposit removal is faster than scar  
 532 filling. In particular shoal margin collapses in secondary channels develop slowly, e.g. tidal flats of 'Brouwer-  
 533 erplaat' (E) and 'Molenplaat' (F), and the less dynamic landward part of the estuary, 'Verdronken Land van  
 534 Saeftinghe' (J). Wiggles indicate effects of neap-spring tidal cycles.

#### 567 4.3.2 Multiple yearly collapses

568 In the third scenario, shoal margin collapses are added after each morphological  
 569 year. Only one collapse could occur at a single shoal, which results in about 5 collapses  
 570 per year equal to field observations of *Van Dijk et al. [2018]*. Our analysis focus specifi-  
 571 cally on the role of multiple shoal margin collapses on the morphodynamics of the sys-  
 572 tem. The shoal margin collapses vary in size and location according to the given rules  
 573 (see method section). After 40 year simulation 227 collapses occurred, i.e., 5.7 per year,  
 574 at 58 locations of various tidal flats (illustrated by contour lines in Figure 8a), eroding a  
 575 total volume of 40 million  $\text{m}^3$ , i.e., 1 million  $\text{m}^3$  per year, which is more than the field  
 576 observations. As shown in previous scenarios the distribution of the disturbance varies  
 577 with location, showing mainly changes in the bed elevation in longitudinal direction, i.e.,  
 578 landward and seaward of the collapse (Figure 8a), whereas collapses near the junctions  
 579 lead to changes in the bed elevation across the channel because of the channel is wider  
 580 and shallower. The total bed volume change at the end of the model run compared to the  
 581 control run is  $4.63 \cdot 10^8 \text{ m}^3$ , in which 20% of the volume is explained by the shoal mar-  
 582 gin collapses. The width-averaged bed level difference between the run with collapses and  
 583 the control run (Figure 8b) illustrates migration of the disturbance in both directions, ex-  
 584 citation of the disturbance over time and also dampening of the disturbance. Furthermore,  
 585 there are some unexplained responses that are not directly associated with the collapses  
 586 itself, such as observed between 25 and 30 km from the Western Scheldt mouth (Fig-  
 587 ure 8b). Because of the number of collapses and the yearly adding of new collapses, the  
 588 effect of a single disturbance is difficult to follow. Most changes occur at the locations  
 589 with several collapses. Because of general incision of the channel at the seaward bound-  
 590 ary, we excluded the seaward effects for further interpretation and conclusions of the role  
 591 of shoal margin collapses as this might be the boundary effect of the model. The total  
 592 eroded and deposited volume is  $2.31 \cdot 10^9 \text{ m}^3$  for the run with collapses and  $2.26 \cdot 10^9 \text{ m}^3$   
 593 for the control run, which suggest the simulation are equally dynamic as only 10.0 mil-  
 594 lion  $\text{m}^3$  of the eroded volume is not explained by the collapsed volume of 40 million  $\text{m}^3$ .

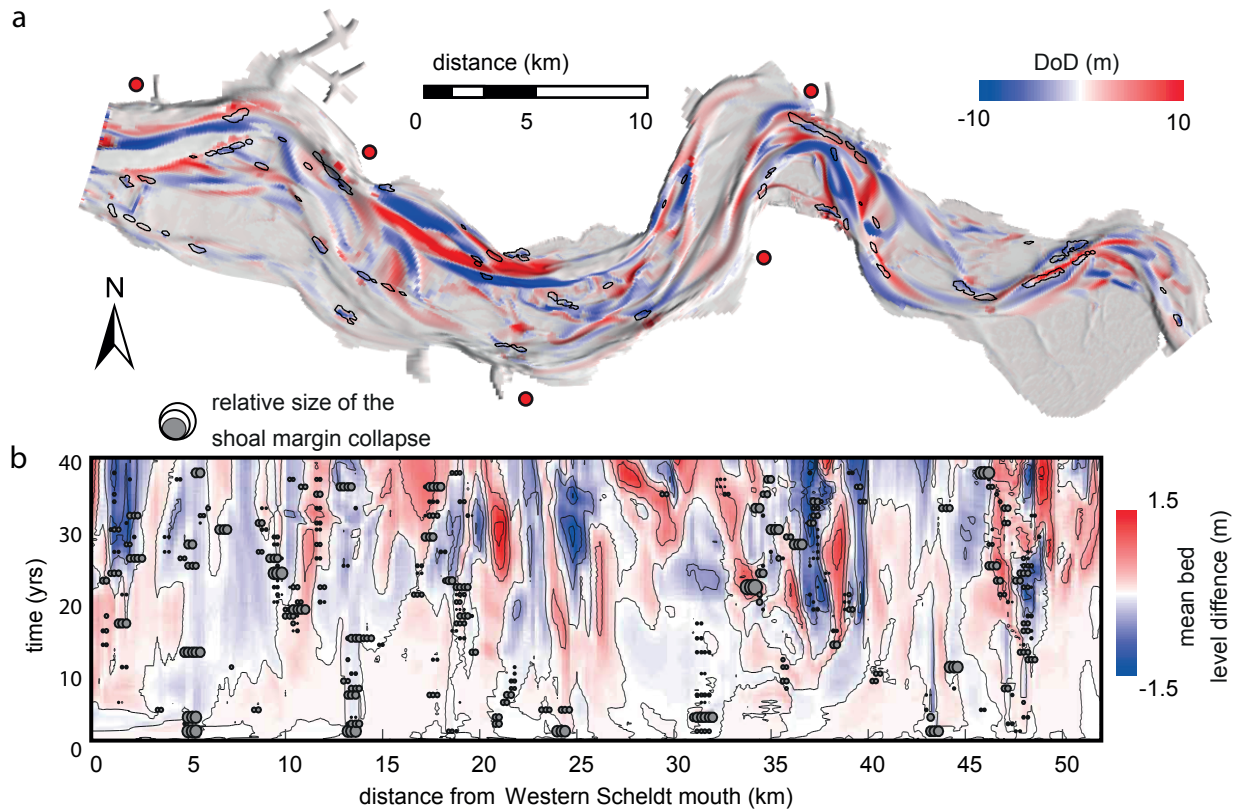


559 **Figure 7.** Effect of multiple initial collapses in the Western Scheldt. a) Elevation difference after 40 years  
 560 between a simulation with and without 10 shoal margin collapses shows that for several locations the per-  
 561 turbation has migrated landward as well as seaward, whereas other collapses hardly migrated over 40 years,  
 562 e.g., locations E and F (see Figure 1a). The colored contour lines show the spatial distribution of the col-  
 563 lapsed material. b) Width-averaged bed elevation difference between the run with and without initial collapses  
 564 shows some migration of the perturbations but mainly shows cumulative excitation effects after two decades.  
 565 c) Spatiotemporal distribution of the collapsed sediment, showing spreading in both seaward and landward  
 566 directions.

595 These volumes indicate that the system does not dynamicise more in the case of including  
 596 shoal margin collapses compared to a control run, which we hypothesized.

#### 602 **4.4 Re-organization of the channel-shoal network by collapses**

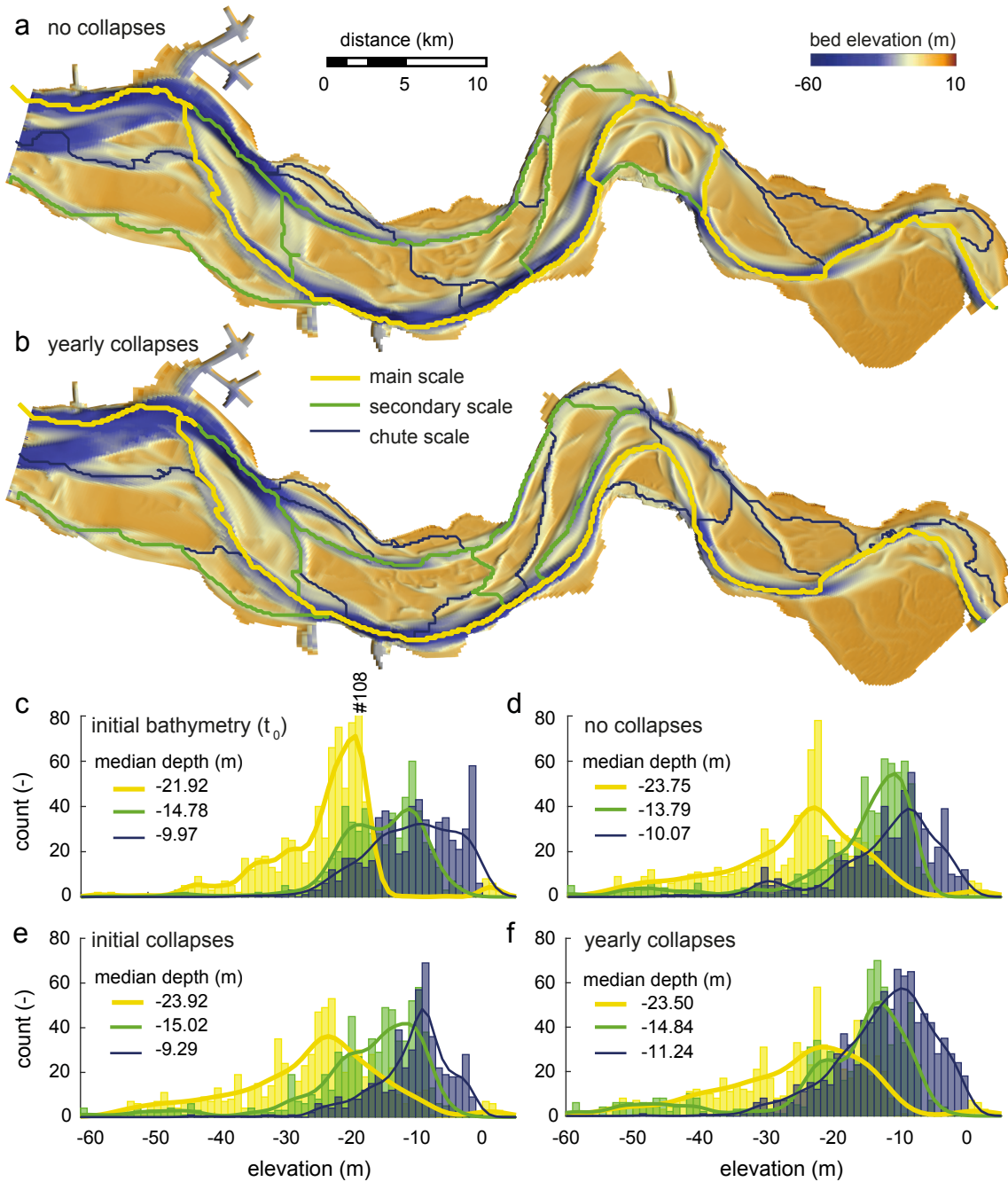
603 The addition of yearly collapses in the model leads to changes in the network struc-  
 604 ture and the scale at which channels are detected as compared to the control run (Fig-  
 605 ure 9a, b). While the main channel location and scale are generally the same between the  
 606 two runs, many of the smaller scale channels are differently identified for the model run  
 607 with yearly collapses. In the control run, less smaller scale channels, i.e. secondary and  
 608 chute, are observed compared to the run with yearly collapses (Figure 9a-b), which means  
 609 there is structural better connectivity among the channels for the model with yearly col-  
 610 lapses. The scale, or sand function volume, at which channels are detected changes be-



597 **Figure 8.** a) Bed elevation difference between a control run and a run with yearly shoal margin collapses  
 598 (indicated by the contour lines) shows that the entire system is modified, especially at junctions forming  
 599 ebb-flood channels (landward of location B and at location H). b) Width-averaged bed elevation difference  
 600 between both runs shows location of incision and deposition that migrates, excites or dampens depending on  
 601 the location of the collapse.

611 tween the runs as well. The shifting of scale is due to the differences in the morphological  
 612 development of the system. In case of the collapses, the secondary channel network shifts  
 613 (Figure 9b), probably because of sediment deposition in the channel which decreases the  
 614 volume of sediment between adjacent channels, causing channels that were identified as  
 615 secondary in the control run to be identified as chute channels in the run with collapses.  
 616 When the volume of sand between channels increases, the opposite is true and  
 617 chute channels become secondary channels.

626 The various channel networks are used to determine the depth distribution of the  
 627 channels. The initial network shows a deep main channel (Table 2, Figure 9c) probably  
 628 due to the dredging activities for maintaining a specific depth of the shipping fairway.  
 629 After 40 years of morphological development, the main channel becomes deeper but the  
 630 variation increases (Table 2), whereas there is an increase of the number of smaller scale  
 631 channels (Figure 9d). Although, we observed some changes in bed elevation between the  
 632 control run and the model with initial 10 collapses (Figure 7), the bed elevation for the  
 633 largest scale of the network is comparable (Figure 9d,e). Major changes are observed  
 634 between the secondary and chute scale channels, the number of chute scale channels in-  
 635 creases for the run with initial collapses, while the depth generally decreases. The depth  
 636 of the secondary channel, however, increases for the run with initial collapses. The bed  
 637 elevation of the main channel and secondary channel are shifting towards each other for



618 **Figure 9.** Networks in (a) the control run without collapses and (b) the scenario with yearly collapses,  
 619 showing that spatial channel shifts and changes in scale of channels after 40 years morphological develop-  
 620 ment. c-f) Depth distributions of the channel networks shows a deep initial main channel (c), which becomes  
 621 shallower when modeled (d). The depth distribution for the run with initial collapses develops towards the  
 622 control run (e), whereas continuous yearly collapses lead to further shallowing of main channel in the estuary  
 623 (f).

624 **Table 2.** Statistics of the mean  $\mu$  and standard deviation  $\sigma$  of the depth for the various runs for all network  
 625 scales.

Scale	$\mu$ (m)				$\sigma$ (m)			
	initial	scenario			initial	Scenario		
		control	2	3		control	2	3
main	-23.91	-26.16	-25.79	-25.73	8.16	10.95	11.13	11.02
secondary	-15.65	-17.41	-17.88	-19.15	7.19	10.87	10.11	11.93
chute	-10.60	-12.23	-10.62	-12.35	6.60	8.00	5.95	7.09

638 the run with yearly collapses, mainly because the mean depth increases faster for the sec-  
 639 ondary channel (Figure 9f). Overall, the system with yearly collapses develops to a system  
 640 with shallower channels because of collapses are mainly in the main-channel, and the sec-  
 641 ondary channels approaches the same depth distribution as the main channel on the long-  
 642 term, whereas the number of chute channels increases.

## 643 5 Discussion

644 We introduced an effective parametrization for the process of shoal margin collapse,  
 645 solely based on the local bed elevation and slope gradient. Here, we discuss how the re-  
 646 sponse of the modeled collapses affects the morphodynamics and how this differs from  
 647 observations. We also consider the implication of shoal margin collapses on perturbing the  
 648 estuarine morphodynamics and compare these with larger perturbations caused by dredg-  
 649 ing and disposal activities.

### 650 5.1 Modeled collapses versus observations

651 The 2014 shoal margin collapse is used to test the near-field effects of a shoal mar-  
 652 gin collapse. This collapse is well studied by *Van Schaick* [2015] by analyzing field mea-  
 653 surements and Delft3D simulations. *Van Schaick* [2015] concluded that some morphody-  
 654 namics of the model differ from the observations [*Mastbergen et al.*, 2016]. According to  
 655 field measurements, sediment deposited from the shoal margin collapse migrates in flood  
 656 direction, while the model outcome suggests sediment transport in ebb direction for the  
 657 bedload. The discrepancy in the direction of the sediment transport could be explained  
 658 by the difference in the tidally averaged flow and tidal asymmetry. The collapsed deposit  
 659 from the 2014 shoal margin collapse is located in that part of the channel where tidally av-  
 660 eraged flow is ebb dominated but almost zero, whereas south from the deposit the tidally  
 661 averaged flow and mean sediment transport suggest transport in flood direction. However,  
 662 the flood current is generally stronger in the channel, which might have led to distribution  
 663 in flood direction instead of the modeled ebb direction. The rate of infilling of erosion  
 664 scars was less in the model compared to field observations. The focus of our study is not  
 665 to calibrate the model to the observed development of the shoal margin collapse of 2014,  
 666 but predict the effect of shoal margin collapses on the large-scale development of the estu-  
 667 ary.

668 The shoal margin collapse parametrization leads to several collapses along the West-  
 669 ern Scheldt Estuary. The location is based on the bed elevation, such that steep slopes col-  
 670 lapses, whereas the collapsed size and volume is randomly drawn from a log-normal dis-  
 671 tribution. Locations for shoal margin collapses (Figure 8a) do vary from the observed lo-  
 672 cations (Figure 1a), probably because for the chosen probability threshold value the num-  
 673 ber of false positives is at least equal to the true positives, meaning that steep high slopes  
 674 that are not susceptible to collapses are included [*Van Dijk et al.*, 2018]. Nonetheless, the

675 collapses are widely distributed on tidal flats that do have collapses over time. Locations  
676 with rapid infilling of the scar relates to locations with multiple collapses, e.g., at Spijker-  
677 plaat (location A) and Ossensisse [location H, *Van Dijk et al.*, 2018]. Our parametrization  
678 differs from earlier attempts to prevent steep slopes of bars in rivers with Delft3D [*Nieuw-*  
679 *boer*, 2012]. *Nieuwboer* [2012] applies two strategies to reduce steep slopes in Delft3D;  
680 1) slope avalanching, and 2) slope slumping, in which avalanching stopped deposition  
681 of sediment on steep slopes and slumping leads to changing steep slopes to equilibrium.  
682 The slope slumping, however, leads to numerically unstable simulations because of large  
683 changes in the water levels. Here, no numerical instabilities were observed, because the  
684 collapses mainly occurred underwater and water depths are higher in the estuary setting  
685 compared to shallow rivers. Furthermore, sediment was not deposited in adjacent cells but  
686 spread in the deeper parts of the channel following the slope of the collapsed shoal.

687 Our parametrization is, however, limited in the prediction of the collapses as the  
688 original probability prediction of *Van den Ham et al.* [2014] includes also variables for  
689 sediment properties, such as grain-size, relative density and the amount of mud layers  
690 [*Mastbergen and Van den Berg*, 2003], whereas we solely calculated with uniform sedi-  
691 ment size. These variations in sediment properties are formed when the channels mi-  
692 grates, forming new shoals on the inner banks whilst collapsing outer banks retreat into  
693 the layer-cake of sand and mud of past shoals and marshes [*Dalrymple and Rhodes*, 1995;  
694 *Van den Berg et al.*, 1996; *Fagherazzi et al.*, 2004]. Spatial information of the stratigraphy  
695 is however lacking for most systems because the limited availability of field data. Even  
696 for the well-studied Western Scheldt a model is used to predict clay availability within the  
697 tidal flats [*Dam*, 2017], but lacks the detailed information. The applied Western Scheldt  
698 schematization includes only a single fraction, but it will be of interest for future studies  
699 to calculate with multiple fractions, especially to construct a subsurface including varia-  
700 tions in sediment properties, e.g., mud [*Braat et al.*, 2017].

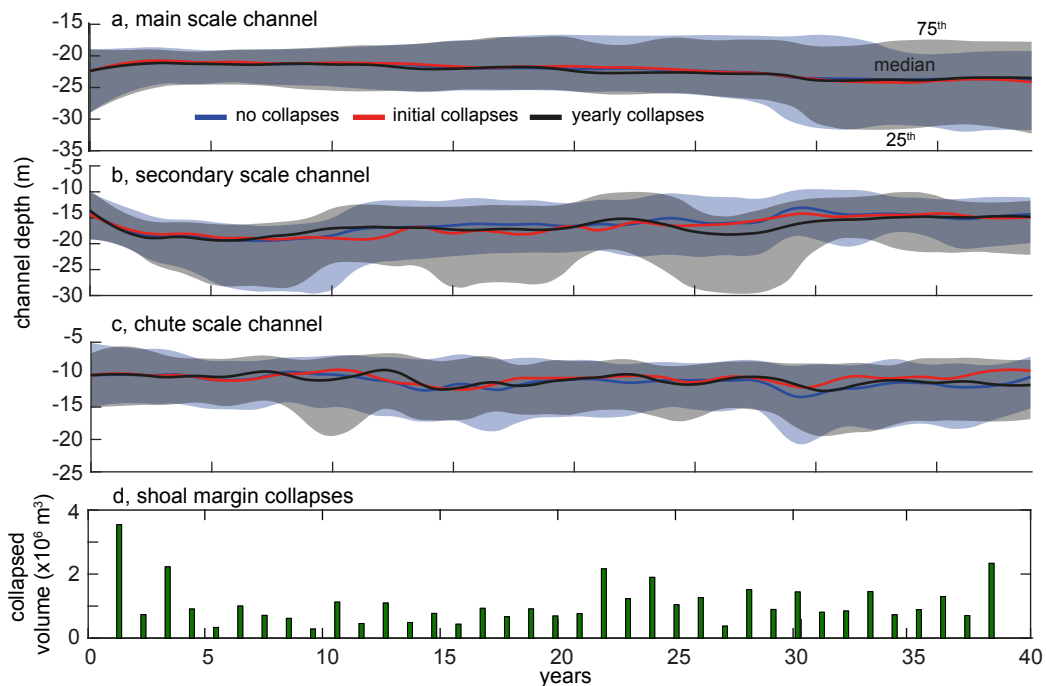
## 701 **5.2 Implications of shoal margin collapse perturbations on the morphodynamics**

702 The rate of sediment removal and the volume of a single collapse determine the  
703 morphodynamics around the collapse. In the less dynamic secondary channels, the sedi-  
704 ment is less spread, so that the collapse has less impact on the channel-shoal morphody-  
705 namics. Small collapses can be seen as noise to the system, while larger collapses can be  
706 seen as a perturbation of the system [*Kleinhaus et al.*, 2015]. The shoal margin collapse  
707 firstly affects the local bed elevation by depositing sediments into the main channel, but  
708 over time this disturbance propagates through the channel network. The findings corre-  
709 spond partly with the conceptual model described by *Schuurman et al.* [2016a] for dis-  
710 turbances in braided rivers. In the estuary however, an adjustment in the channel leads to  
711 adjustments in downstream and upstream direction. The dominant direction depends on  
712 if the channel is ebb or flood dominant. The migration rate is low for the disturbance but  
713 larger than changes of the shoals (tidal flats) themselves, which are more or less fixed at  
714 their location [*Leuven et al.*, 2018b].

715 The initial 10 collapses show that the perturbations lead to excitation of the differ-  
716 ence in bed elevation compared to a control run on the long-term. Specifically, the bed el-  
717 evation difference between the runs increases rapidly after 20 years. Where after 40 years  
718 of morphological development, the modeled bed elevation difference between the con-  
719 trol run and the run with initial collapses is only explained by less than 10% of the ini-  
720 tial collapsed volume. In the case for the scenario with yearly collapse, the modeled bed  
721 elevation difference is explained by 20% of the collapsed volume, probably this percent-  
722 age is less because the effect from the disturbances are still growing, the perturbations are  
723 less effective because of some smaller collapses, or small perturbations are overprinted by  
724 larger ones. In case of the initial collapses, the perturbation grows over time but besides  
725 some deepening of the secondary channel the channel network remains the same. On the

726 other hand, the yearly collapses change the course of the secondary and main channel at a  
 727 few locations (see Supplementary Animation 1).

728 Shoal margin collapses perturb the estuary differently depending on the location of  
 729 the collapse within the channel network. In general, the shoal margin collapses change  
 730 the channel-shoal network by shallowing of the major channels and forming new smaller  
 731 channels on the tidal flats. The network tool provides a network at the final timestep (Fig-  
 732 ure 9), illustrating the overall changes between the control run and yearly collapse but did  
 733 not illustrate changes that can be linked to the collapses themselves. Analysis of the chan-  
 734 nel depth for the various scales in time shows that the variation in channel depth increases  
 735 in time, except for the secondary channels (Figure 10). The channel network changes part  
 736 of the main channel into the secondary channel within the first 5 years for all runs, so that  
 737 the secondary channel deepens and the main channel becomes shallower (Figure 10a, b).  
 738 The collapses in the scenario with yearly collapses mainly affect the secondary and chute  
 739 scale channel networks, which deviates from the control run (Figure 10b, c). A few col-  
 740 lapse events can be directly related with changes in the channel network depth. For ex-  
 741 ample, the collapses in year 22 results in shallowing of the secondary scale channel (Fig-  
 742 ure 10b). Changes in the depth of the larger channel network scales are not directly af-  
 743 fected by the collapses but might be the result of multiple collapses that affected the chute  
 744 scale channel networks. For example, the shallowing of the secondary scale channel net-  
 745 work after 10 years corresponds to a deepening of the chute scale channel network that  
 746 occurred a year before (Figure 10b, c).



747 **Figure 10.** Depth over time for the three model runs illustrating an increasing variation in depth for the  
 748 various network scales. a) Median depth for the main channel network over time shows minor differences  
 749 with the control run. b) Secondary channel network deviates after 10 years for the run with yearly collapses.  
 750 c) Chute channel network shows faster response time to collapses. Shading indicates quartiles. Considerable  
 751 deviations are observed for the yearly collapses at 9, 18 and 30 years and for the initial collapses at 13, 27 and  
 752 36 years. d) Time and volume of shoal margin collapses.

753 The shoal margin collapses does not dynamicise the morphodynamics as we hypoth-  
754 esized, but does change the estuary morphodynamics compared to a control run without  
755 collapses. The most interesting responses from the collapses on the channel-shoal mor-  
756 phodynamics is observed near junctions (sills, Figures 7-8), corresponding to the over-  
757 lapping sediment circulation cells [Wang *et al.*, 1995], the part with less bruto sediment  
758 transport but morphodynamic active part of the Western Scheldt [Van Dijk *et al.*, 2018]  
759 observed from DEM of differences for the last decades [Grasmeijer *et al.*, 2013] but not  
760 on the long-term sediment balance of the Western Scheldt that shows the development of  
761 channel-shoals for the period 1860-1955 [Dam, 2017]. This suggests that dynamics of the  
762 shoals have been decreased in the last decades and that perturbations, such as shoal mar-  
763 gin collapses, efficiently are removed in the main and secondary channels and only affect  
764 the development at the shallower sills, channel junctions. The mean bed elevation at the  
765 junction does increase even when there is almost no direct deposition of the collapsed sed-  
766 iment (Figure 7b, c). A reason could be that collapsed sediment is spread over a larger/  
767 wider distance, however the role of the junction is significant as this leads to excitation of  
768 the disturbance. Disturbances at the junction change the flow direction towards the suc-  
769 cessive shoal, like the successive bifurcation in a braided river [Schuurman *et al.*, 2016a],  
770 but also the flow direction towards the shoal itself as the tidally averaged flow circulates,  
771 i.e., marco cell, around the shoal (Figure 1b). This means that disturbances near a junc-  
772 tion would have a larger effect on the channel-shoal morphodynamics. For example, the  
773 collapses near Borssele (location B) and at Ossennisse (location H) result in larger differ-  
774 ences from the control run. In the field, however, the junction (sill) is well managed as  
775 this is part of the shipping fairway, and therefore its depth is maintained by dredging ac-  
776 tivities [Verbeek *et al.*, 1998], which means that the role of collapses cannot be observed  
777 in the field.

778 The role of the shoal margin collapses might affect the estuary differently com-  
779 pared to dredging and dumping activities, which is conducted to deepen the main chan-  
780 nel. Dredging activities at the toe of the 'Platen van Ossennisse' ['Drempel van Hansweert'  
781 *Groenewoud*, 1997] might lead to deepening and increase the number of shoal margin col-  
782 lapses in the field, which is not included in our simulations. In this study, we have not  
783 included dredging and dumping, which would affect our finding. For example, dredging  
784 and dumping studies in the Western Scheldt estuary show that the dumping strategies  
785 affect the estuary differently. Till 1970, dredging was restricted to maintain depths for  
786 navigation in the main ebb channel, and the dredged sediment was disposed in the flood  
787 (secondary) channels because of the longer period before reaching the main ebb channel  
788 [Meersschaut *et al.*, 2004]. This is comparable to our findings that shoal margin collapse  
789 deposits in the flood channels take longer to spread towards the junction, i.e., sill, because  
790 of the lower sediment transport. Because of continuous disposal of dredge volumes in  
791 the secondary flood channels aggradation was observed in these channels [Meersschaut  
792 *et al.*, 2004], which formed a threat for the existence of the multiple channel network, a  
793 new flexible disposal strategy was introduced to steer the development of channels and  
794 shoals [Meersschaut *et al.*, 2004; Vos *et al.*, 2009]. This flexible disposal strategy encom-  
795 passes redistributing sediment to feed areas that are eroding too much, e.g., the western tip  
796 of the 'Plaat van Walsoorden' (location I). Although, the extensive monitoring and model  
797 study of the flexible disposal strategy [Vos *et al.*, 2009; IMDC, 2011, 2015], it will be of  
798 interest to test the effect on the long-term channel network of various dredging-disposal  
799 strategies and the stability of the multiple channel network [Wang, 2015]. Dredged vol-  
800 umes are 10 times larger compared to shoal margin collapses in the Western Scheldt we  
801 would argue that therefore the role of shoal margin collapses on the morphodynamics in  
802 the Western Scheldt is hardly observable. The role of the shoal margin collapses might  
803 affect the estuary differently compared to dredging and dumping activities, which is con-  
804 ducted to deepen the main channel. Dredging activities at the toe of the 'Platen van Os-  
805 senisse' ['Drempel van Hansweert' *Groenewoud*, 1997] might lead to deepening and in-  
806 crease the number of shoal margin collapses in the field, which is not included in our sim-  
807 ulations. In this study, we have not included dredging and dumping, which would affect

808 our finding. For example, dredging and dumping studies in the Western Scheldt estuary  
809 show that the dumping strategies affect the estuary differently. Till 1970, dredging was  
810 restricted to maintain depths for navigation in the main ebb channel, and the dredged sed-  
811 iment was disposed in the flood (secondary) channels because of the longer period be-  
812 fore reaching the main ebb channel [Meersschaut *et al.*, 2004]. This is comparable to our  
813 findings that shoal margin collapse deposits in the flood channels take longer to spread  
814 towards the junction, i.e., sill, because of the lower sediment transport. Because of con-  
815 tinuous disposal of dredge volumes in the secondary flood channels aggradation was ob-  
816 served in these channels [Meersschaut *et al.*, 2004], which formed a threat for the exis-  
817 tence of the multiple channel network, a new flexible disposal strategy was introduced to  
818 steer the development of channels and shoals [Meersschaut *et al.*, 2004; Vos *et al.*, 2009].  
819 This flexible disposal strategy encompasses redistributing sediment to feed areas that are  
820 eroding too much, e.g., the western tip of the ‘Plaat van Walsoorden’ (location I). Al-  
821 though, the extensive monitoring and model study of the flexible disposal strategy [Vos  
822 *et al.*, 2009; IMDC, 2011, 2015], it will be of interest to test the effect on the long-term  
823 channel network of various dredging-disposal strategies and the stability of the multiple  
824 channel network [Wang, 2015]. Dredged volumes are 10 times larger compared to shoal  
825 margin collapses in the Western Scheldt we would argue that therefore the role of shoal  
826 margin collapses on the morphodynamics in the Western Scheldt is hardly observable.

## 827 **6 Conclusions**

828 Detailed analysis of the 2014 shoal margin collapse shows that the hydrological  
829 and morphological processes around the shoal margin collapse are affecting water lev-  
830 els and sediment transport direction. Model results show that single shoal margin col-  
831 lapses only affect the local dynamics in longitudinal direction and dampen out within a  
832 year when volumes are small. The extent of far-field effects is sensitive to the grain-size  
833 of the deposit, where finer sediments are transported further away and settles on the sides  
834 while larger grains are hardly entrained and only eroded during the stronger flood flow.  
835 The location of the deposit across the channel matters for disturbing the region around  
836 the collapse, where sediment transport is dominantly following the tidally averaged flow  
837 but coarser sediment follows the stronger flood flow. The perturbation by the shoal mar-  
838 gin collapses increases channel migration rate, as the deposited sediment pushes the flow  
839 against the banks. These results imply that disturbances caused by dredging and dumping  
840 may likewise affect the dynamics of channel junctions as well, because dredging volumes  
841 are at least 10 times larger than the collapsed volumes.

842 We presented a parametrization for shoal margin collapses and coupled this to the  
843 Delft3D model, so that effects of multiple yearly collapses of various sizes on the mor-  
844 phodynamics could be tested. We found that near-field morphodynamics in the channel  
845 are slightly affected at a timescale of a year due to increasing bed elevation and changing  
846 water levels, but far-field effects such as the tidally averaged flow vectors are negligible  
847 affected by the collapses. When larger disturbances reach the seaward or landward junc-  
848 tion at tidal channel junctions over a longer time span, the bed elevation at the junction  
849 increases on average and decrease the hydraulic geometry of the channel junctions. Here,  
850 the perturbation affects the morphology in longitudinal as well as transverse direction, and  
851 affect the channel network on a longer term when the flow and sediment distributions into  
852 the multiple channels are shifted. The initial collapses have no effect on the long-term  
853 channel-shoal morphodynamics, although bed elevation difference is only for 10% ex-  
854 plained by the collapsed volume. The yearly collapses resulted in a shallowing of the main  
855 channel as they mostly occur along the main channel, and change the channel networks  
856 at the various scales. The secondary scaled channels become deeper, whereas the number  
857 of the chute scale channels increases when the system gets generally shallower. We con-  
858 clude that multiple yearly collapses are changing the channel-shoal morphodynamics in  
859 estuaries, but that the role of the collapses is limited for heavily dredged systems such as

860 the Western Scheldt. On the other hand, estuaries that are not intensively dredged may not  
861 develop oversteepened bar margins with frequent shoal margin collapses.

## 862 **Acknowledgments**

863 WMvD and MGK were supported by the Dutch Technology Foundation TTW (grant STW-  
864 Vici-016.140.316/13710 to MGK), which is part of the Netherlands Organisation for Sci-  
865 entific Research (NWO). MH and MGK were supported by the European Research Council  
866 (ERC Consolidator agreement 647570 to MGK). We gratefully acknowledge Marco  
867 Schrijver (Rijkswaterstaat), Dick Mastbergen, Marcel Taal (Deltares) and Jelmer Clev-  
868 eringa (Arcadis) for insightful discussions. Reviewers will be acknowledged. The data  
869 used are listed in the references, figures and supplements.

## 870 **References**

- 871 Ahktar, M. P., N. Sharma, and C. S. P. Ojha (2011), Braiding process and bank erosion  
872 in the Brahmaputra River, *International Journal of Sedimentary Research*, 26, doi:  
873 10.1016/S1001-6279(12)60003-1.
- 874 Ashworth, P. J., and J. Lewin (2012), How do big rivers come to be different?, *Earth-*  
875 *Science Reviews*, 114, 84–107, doi:10.1016/j.earscirev.2012.05.003.
- 876 Baar, A. W., J. De Smit, W. S. J. Uijtewaai, and M. G. Kleinhans (2018), Sediment trans-  
877 port of fine sand to fine gravel on transverse bed slopes in rotating annular flume exper-  
878 iments, *Water Resources Research*, p. 10.1002/2017WR020604.
- 879 Beinssen, K., D. T. Neil, and D. R. Mastbergen (2014), Field observations of retrogressive  
880 breach failure at the two tidal inlets in Queensland, Australia, *Australian Geomechanics*,  
881 49(3), 55–64.
- 882 Bolle, A., Z. B. Wang, C. Amos, and J. De Ronde (2010), The influence of changes in  
883 tidal asymmetry on residual sediment transport in the Western Scheldt, *Continental*  
884 *Shelf Research*, 30, 871–882, doi:10.1016/j.csr.2010.03.001.
- 885 Braat, L., T. Van Kessel, J. R. F. W. Leuven, and M. G. Kleinhans (2017), Effects of mud  
886 supply on large-scale estuary morphology and development over centuries to millennia,  
887 *Earth Surface Dynamics Discussion*, 5, 617–652, doi:10.5194/esurf-5-617-2017.
- 888 Cancino, L., and R. Neves (1999), Hydrodynamic and sediment suspension modelling  
889 in estuarine systems, *Journal of Marine Systems*, 22, 117–131, doi:10.1016/S0924-  
890 7963(99)00036-6.
- 891 Canestrelli, A., A. Spruyt, B. Jagers, R. Slingerland, and M. Borsboom (2016), A mass-  
892 conservative staggered immersed boundary model for solving the shallow water equa-  
893 tions on complex geometries, *International Journal for Numerical Methods in Fluids*, 81,  
894 151–177, doi:10.1002/flid.4180.
- 895 Coleman, J. M. (1969), Brahmaputra River: channel processes and sedimentation, *Sedi-*  
896 *mentary Geology*, 3, 129–239, doi:10.1016/0037-0738(69)90010-4.
- 897 Crosato, A., and M. S. Saleh (2011), Numerical study on the effects of floodplain vegeta-  
898 tion on river planform style, *Earth Surface Processes and Landforms*, 36, 711–720.
- 899 Dalrymple, R., and R. Rhodes (1995), Estuarine dunes and bars, in *Developments*  
900 *in Sedimentology*, vol. 53, pp. 359–422, Elsevier, New York, doi:10.1016/S0070-  
901 4571(05)80033-0.
- 902 Dam, G. (2013), Harde lagen Westerschelde (in Dutch), *Tech. rep.*, International Marine &  
903 Dredging Consultants.
- 904 Dam, G. (2017), Lange-termijn sedimentbalans Westerschelde (in Dutch), *Tech. rep.*,  
905 SVASEK hydraulics.
- 906 Darby, S. E., A. M. Alabyan, and M. J. Van de Wiel (2002), Numerical simulation of  
907 bank erosion and channel migration in meandering rivers, *Water Resources Research*,  
908 38, doi:10.1029/2001WR000602.

- 909 De Vriend, H. J., Z. B. Wang, T. Ysebaert, P. M. J. Herman, and P. Ding (2011), Eco-  
910 morphological problems in the Yangtze Estuary and the Western Scheldt, *Wetlands*, *31*,  
911 1033–1042, doi:10.1007/s13157-011-0239-7.
- 912 Deltares (2009), *Delft3D-FLOW User Manual, Simulation of Multi-Dimensional Hydro-*  
913 *dynamic Flows and Transport Phenomena, Including Sediments*, Deltares, Delft, The  
914 Netherlands.
- 915 Dunbar, J. B., V. H. Torrey, and L. D. Wakeley (1999), A case history of embankment  
916 failure: geological and geotechnical aspects of the Celotex levee failure, New Orleans,  
917 Louisiana, *Technical report*, US Army Corps of Engineers, Vicksburg, Mississippi,  
918 USA.
- 919 Fagherazzi, S., E. J. Gabet, and D. J. Furbish (2004), The effect of bidirectional flow on  
920 tidal channel planforms, *Earth Surface Processes and Landforms*, *29*, 295–309, doi:  
921 10.1002/esp.1016.
- 922 Grasmeyer, B., G. Dam, and M. Taal (2013), Actualisatierapport Delft3D Schelde-  
923 estuarium (in Dutch), *Tech. rep.*, International Marine & Dredging Consultants.
- 924 Grenfell, M. C. (2012), Chute channels in large, sand-bed meandering rivers, Ph.D. the-  
925 sis, University of Exeter.
- 926 Groenewoud, M. D. (1997), Modelling morfodynamisch gedrag van de Drempel van  
927 Hansweert (in Dutch), Master's thesis, TU Delft.
- 928 Gruijters, S. H. L. L., J. Schokker, and J. G. Veldkamp (2004), Kartering moeilijk erodeer-  
929 bare lagen in het Schelde estuarium (in Dutch), *rapport NITG 03213B1208*, TNO.
- 930 IMDC (2011), Bepaling van de T0 situatie voor flexibel storten (in Dutch), *Tech. rep.*, In-  
931 ternational Marine & Dredging Consultants.
- 932 IMDC (2015), Deelopdracht 8 - Maandrapport plaatrandstortingen augustus - september  
933 2015 (in Dutch), *Tech. rep.*, International Marine & Dredging Consultants, Antwerp,  
934 Belgium.
- 935 Jerolmack, D. J., and C. Paola (2010), Shredding of environmental signals by sediment  
936 transport, *Geophysical Research Letters*, *37*(19), doi:10.1029/2010GL044638, 119401.
- 937 Jeuken, M. C. J. L. (2000), On the morphologic behaviour of the tidal channels in the  
938 Westerschelde estuary, Ph.D. thesis, Universiteit Utrecht.
- 939 Khan, N. I., and A. Islam (2003), Quantification of erosion patterns in the Brahmaputra-  
940 Jamuna River using geographical information system and remote sensing techniques,  
941 *Hydrological Processes*, *17*, doi:10.1002/hyp.1173.
- 942 Kleinhans, M. G. (2010), Sorting out river channel patterns, *Progress in Physical Geogra-*  
943 *phy*, *34*, 287–326, doi:10.1177/0309133310365300.
- 944 Kleinhans, M. G., C. Braudrick, W. M. Van Dijk, W. I. Van de Lageweg, R. Teske, and  
945 M. Van Oorschot (2015), Swiftness of biomorphodynamics in Lilliput- to Giant-sized  
946 rivers and deltas, *Geomorphology*, *244*, 56–73, doi:10.1016/j.geomorph.2015.04.022.
- 947 Kleinhans, M. G., M. Kreveld, T. Ophelders, W. Sinke, B. Speckmann, and K. Verbeek  
948 (2017), Computing representative networks for braided rivers, in *33rd International Sym-*  
949 *posium on Computational Geometry (SoCG 2017), Leibniz International Proceedings*  
950 *in Informatics (LIPIcs)*, vol. 77, edited by B. Aronov and M. J. Katz, pp. 48:1–48:16,  
951 Schloss Dagstuhl–Leibniz-Zentrum fuer Informatik, doi:10.4230/LIPIcs.SoCG.2017.48.
- 952 Laury, R. L. (1971), Stream bank failure and rotational slump: preservation and signifi-  
953 cance in the geologic record, *Geological Society of America Bulletin*, *82*, 1251–1266.
- 954 Leuven, J. R. F. W., T. De Haas, L. Braat, and M. G. Kleinhans (2018a), Topographic  
955 forcing of tidal sand bar patterns for irregular estuary planforms, *Earth Surface Pro-*  
956 *cesses and Landforms*, *43*(1), 172–186, doi:10.1002/esp.4166.
- 957 Leuven, J. R. F. W., L. Braat, W. M. van Dijk, T. De Haas, J. Cleveringa, and M. G.  
958 Kleinhans (2018b), Growing forced bars determine non-ideal estuary planform, *Earth-*  
959 *ArXiv*, doi:10.17605/OSF.IO/HJ27M.
- 960 Mastbergen, D. R., and R. Schrijvershof (2016), Sedimentatiepatronen Plaat van Walsoor-  
961 den na plaatval 22 juli 2014 (in Dutch), *Tech. rep.*, Deltares, deltares.

- 962 Mastbergen, D. R., and J. H. Van den Berg (2003), Breaching in fine sands and the gener-  
 963 ation of sustained turbidity currents in submarine canyons, *Sedimentology*, 50(4), 625–  
 964 637, doi:10.1046/j.1365-3091.2003.00554.x.
- 965 Mastbergen, D. R., G. A. Van den Ham, M. Cartigny, A. Koelewijn, M. De Kleine,  
 966 J. Hizett, M. Azpiroz, and A. Vellinga (2016), Multiple flow slide experiment in the  
 967 Westerschelde Estuary, The Netherlands, in *Submarine Mass Movements and Their Con-*  
 968 *sequences, 7th Int. Symp, Advances in Natural and Technological Hazards Research*,  
 969 vol. 41, edited by G. Lamarche, J. Mountjoy, S. Bull, T. Hubble, S. Krastel, E. Lane,  
 970 A. Micallef, L. Moscardelli, C. Mueller, I. Pecher, and S. Woelz, pp. 241–249, Springer  
 971 International Publishing, Wellington, New Zealand, doi:10.1007/978-3-319-20979-1.
- 972 Maximova, T., S. Ides, J. Vanlede, T. De Mulder, and F. Mostaert (2009a), Verbetering 2D  
 973 randvoorwaardenmodel. Deelrapport 3: kalibratie bovenlopen (in Dutch), *WL rapporten*  
 974 *753\_09*, Flanders Hydraulics Research, Antwerp, Belgium.
- 975 Maximova, T., S. Ides, T. De Mulder, and F. Mostaert (2009b), LTV O & M thema Veiligheid - Deelproject 1: Verbetering hydrodynamisch NeVla model ten behoeve van scenario-analyse (in Dutch), *WL rapporten 756\_05*, Flanders Hydraulics Research & Deltares, Antwerp, Belgium.
- 979 Maximova, T., S. Ides, T. De Mulder, and F. Mostaert (2009c), Verbetering randvoorwaardenmodel. Deelrapport 4: Extra aanpassingen Zeeschelde (in Dutch), *WL rapporten 753\_09*, Flanders Hydraulics Research, Antwerp, Belgium.
- 982 Meersschaut, Y. M. A., W. R. Parker, J. J. Peters, and Y. M. G. Plancke (2004), A dredging and disposal strategy for managing the Western Scheldt's morphology and ecology, in *WODCON XVII: Dredging in a Sensitive Environment*.
- 985 Nicholas, A. P. (2013a), Morphodynamic diversity of the world's largest rivers, *Geology*, 41(4), 475–478, doi:10.1130/G34016.1.
- 987 Nicholas, A. P. (2013b), Modelling the continuum of river channel patterns, *Earth Surface Processes and Landforms*, 38, 1187–1196, doi:10.1029/2010JF001774.
- 989 Nieuwboer, B. (2012), Numerical modelling of Colorado sandbar growth, Master's thesis, TU Delft.
- 991 Olsen, N. R. (2003), Three-dimensional CFD modelling of self-forming meandering channel, *Journal of Hydraulic Engineering*, 129, 366–372, doi:10.1061/(ASCE)0733-9429(2003)129:5(366).
- 994 Paola, C., P. Heller, and C. Angevine (1992), The large-scale dynamics of grain-size variation in alluvial basins. I: Theory, *Basin Res.*, 4, 73–90.
- 996 Roelvink, J. A. (2006), Coastal morphodynamic evolution techniques, *Coastal Engineering*, 53(2–3), 277–287, doi:10.1016/j.coastaleng.2005.10.015.
- 998 Schrijvershof, R., and J. Vroom (2016), Effecten van realistische (extreme) stortstrategieën in de Westerschelde (in Dutch), *Tech. rep.*, Deltares.
- 1000 Schuurman, F., M. G. Kleinhans, and W. A. Marra (2013), Physics-based modeling of large braided sand-bed rivers: bar pattern formation, dynamics, and sensitivity, *Journal of Geophysical Research – Earth Surface*, 118, 2509–2527, doi:10.1002/2013JF002896.
- 1002 Schuurman, F., M. G. Kleinhans, and H. Middelkoop (2016a), Network response to disturbances in large sand-bed braided rivers, *Earth Surface Dynamics*, 4, 25–45, doi:10.5194/esurf-4-25-2016.
- 1006 Schuurman, F., Y. Shimizu, T. Iwasaki, and M. G. Kleinhans (2016b), Dynamic meandering in response to upstream perturbations and floodplain formation, *Geomorphology*, 253, 94–109, doi:10.1016/j.geomorph.2015.05.039.
- 1009 Silvis, F., and M. B. De Groot (1995), Flow slide in the Netherlands: experience and engineering practice, *Canadian Geotechnical Journal*, 32, 1086–1092, doi:10.1139/t95-107.
- 1011 Simon, A., and A. J. C. Collinson (2002), Quantifying the mechanical and hydrologic effects of riparian vegetation on streambank stability, *Earth Surface Processes and Landforms*, 27(5), 527–546, doi:10.1002/esp.325.
- 1014 Torrey, V. H. (1995), Flow slides in Mississippi riverbanks, in *River, Coastal and Shoreline Protection-Erosion Control. Using Riprap and Armourstone*, edited by C. R. Thorne,
- 1015

- 1016 S. R. Abt, B. J. Barendt, S. T. Maynard, and K. W. Pilarczyk, pp. 361–377, Wiley,  
1017 Chichester.
- 1018 Van de Lageweg, W. I., W. M. Van Dijk, A. W. Baar, J. Rutten, and M. G. Kleinhans  
1019 (2014), Bank pull or bar push: What drives scroll-bar formation in meandering rivers?,  
1020 *Geology*, 42(4), 319–322, doi:10.1130/G35192.1.
- 1021 Van den Berg, J. H., C. J. L. Jeuken, and A. J. F. Van der Spek (1996), Hydraulic pro-  
1022 cesses affecting the morphology and evolution of the Western Scheldt estuary, in *Estu-  
1023 arine Shores*, edited by K. F. Nordstrom and C. T. Roman, pp. 157–184.
- 1024 Van den Berg, J. H., A. Van Gelder, and D. R. Mastbergen (2002), The importance of  
1025 breaching as a mechanism of subaqueous slope failure in fine sand, *Sedimentology*,  
1026 49(1), 81–95, doi:10.1111/j.1525-139X.2006.00168.x-i1.
- 1027 Van den Berg, J. H., A. W. Martinius, and R. Houthuys (2017), Breaching-related tur-  
1028 bidites in fluvial estuarine channels: Examples from outcrop and core and implications  
1029 to reservoir models, *Marine and Petroleum Geology*, 82, 178–205.
- 1030 Van den Ham, G. A., M. B. De Groot, and D. R. Mastbergen (2014), A semi-empirical  
1031 method to assess flow-slide probability, in *Submarine mass movements and their conse-  
1032 quences*, vol. 37, edited by S. Krastel, J.-H. Behrmann, D. Volker, M. Stipp, C. Berndt,  
1033 R. Urgeles, J. Chaytor, K. Huhn, M. Strasser, and C. B. Harbitz, Advances in Natural  
1034 and Technological Hazards Research, Springer International Publishing Switzerland, doi:  
1035 10.1007/978-3-319-00972-8.
- 1036 Van der Wegen, M., and J. A. Roelvink (2012), Reproduction of estuarine bathymetry by  
1037 means of a process-based model: Western Scheldt case study, the Netherlands, *Geomor-  
1038 phology*, 179, 152–167, doi:10.1016/j.geomorph.2012.08.007.
- 1039 Van Dijk, W. M., F. Schuurman, W. I. Van de Lageweg, and M. G. Kleinhans (2014),  
1040 Bifurcation instability determines chute cutoff development in meandering gravel-bed  
1041 rivers, *Geomorphology*, 213, 277–291, doi:10.1016/j.geomorph.2014.01.018.
- 1042 Van Dijk, W. M., D. R. Mastbergen, G. A. Van de Ham, and M. G. Kleinhans (2018),  
1043 Probability and causes of shoal margin collapses in a sandy estuary, *Earth Surface Pro-  
1044 cesses and Landforms*, doi:10.1002/esp.4395.
- 1045 Van Rijn, L. C. (2007a), Unified view of sediment transport by currents and waves, i: Ini-  
1046 tiation of motion, bed roughness, and bed-load transport, *Journal of Hydraulic Engineer-  
1047 ing*, 133(6), 649–667.
- 1048 Van Rijn, L. C. (2007b), Unified view of sediment transport by currents and waves, ii:  
1049 Suspended transport, *Journal of Hydraulic Engineering*, 133(6), 668–689.
- 1050 Van Schaick, S. (2015), Morphological development after the July 2014 flow slide on the  
1051 tidal flat of Walsoorden in the Western Scheldt, Master's thesis, Delft University of  
1052 Technology.
- 1053 Verbeek, H., F. T. G. Tank, and M. D. Groenewoud (1998), Drempels in de Westerschelde  
1054 (in Dutch), *Tech. rep.*, Rijksinstituut voor kust en zee/RIKZ.
- 1055 Vos, G., Y. Plancke, S. Ides, T. De Mulder, and F. Mostaert (2009), Sediment relocation to  
1056 shallow water near Walsoorden sandbar. Alternative relocation strategy Westerschelde.,  
1057 *Wl rapporten*, Waterbouwkundig Laboratorium, Antwerp, Belgium.
- 1058 Vroom, J., P. L. M. De Vet, and J. J. Van der Werf (2015), Validatie waterbeweging  
1059 Delft3D NeVla model Westerscheldemonding (in Dutch), *Tech. rep.*, Deltares.
- 1060 Wang, Z., R. Fokkink, M. de Vries, and A. Langerak (1995), Stability of river bifurcations  
1061 in 1D morphodynamic models, *Journal of Hydraulic Research*, 33(6), 739–750.
- 1062 Wang, Z. B. (2015), Sustainability of the multi-channel system in the Westerschelde under  
1063 influence of dredging and disposal, in *Scheldt Estuary, physics and integrated manage-  
1064 ment*, pp. 65–70, IAHR.
- 1065 Wang, Z. B., A. Langerak, and R. J. Fokkink (1999), Simulation of long-term morpholog-  
1066 ical development in the Western Scheldt, in *River, Coastal and Estuarine Morphodynam-  
1067 ics*, pp. 367–376.
- 1068 Whipple, K. X., and G. E. Tucker (1999), Dynamics of the stream-power river inci-  
1069 sion model: Implications for height limits of mountain range, landscape response

- 1070 timescales, and research needs, *Journal of Geophysical Research - Solid Earth*, 104(B2),  
1071 17,661–17,674, doi:10.1029/1999JB900120.
- 1072 Wilderom, M. H. (1961), Tussen afsluitdammen en deltadijken (in dutch), *Tech. rep.*, Rijk-  
1073 swaterstaat, Vlissingen, The Netherlands.
- 1074 Wilderom, M. H. (1972), Plaatvallen (in dutch), *OTAR*, 57(7), 288–305.
- 1075 Wilderom, M. H. (1979), Resultaten van het vooroveronderzoek langs de Zeeuwse  
1076 stromen (in Dutch), *Tech. rep.*, Rijkswaterstaat, nota 75.2.
- 1077 Winterwerp, J. C., M. C. J. L. Jeuken, M. J. F. Stive, and H. J. De Vriend (2000), Lange  
1078 termijnvisie Westerschelde - Cluster Morfologie (in Dutch), *Tech. rep.*, WL Delft Hy-  
1079 draulics.
- 1080 Xu, J. (1997), Evolution of mid-channel bars in a braided river and complex re-  
1081 sponse to reservoir construction: an example from the middle Hanjiang River,  
1082 China, *Earth Surface Processes and Landforms*, 22, doi:10.1002/(SICI)1096-  
1083 9837(199710)22:10<953::AIDESP789>3.0.CO;2-S,.